PHYSICAL REVIEW C **91**, 024301 (2015)

Beyond-mean-field study of elastic and inelastic electron scattering off nuclei

J. M. Yao,[1,2,*] M. Bender,[3,4] and P.-H. Heenen[1]

[1] *Physique Nucléaire Théorique, Université Libre de Bruxelles, C.P. 229, B-1050 Bruxelles, Belgium*
[2] *School of Physical Science and Technology, Southwest University, Chongqing, 400715, China*
[3] *Université de Bordeaux, Centre d'Etudes Nucléaires de Bordeaux Gradignan, UMR5797, F-33175 Gradignan, France*
[4] *CNRS/IN2P3, Centre d'Etudes Nucléaires de Bordeaux Gradignan, UMR5797, F-33175 Gradignan, France*

(Received 9 October 2014; published 3 February 2015)

Background: Electron scattering provides a powerful tool to determine charge distributions and transition densities of nuclei. This tool will soon be available for short-lived neutron-rich nuclei.

Purpose: Beyond-mean-field methods have been successfully applied to the study of excitation spectra of nuclei in the whole nuclear chart. These methods permit determination of energies and transition probabilities starting from an effective in-medium nucleon-nucleon interaction but without other phenomenological ingredients. Such a method has recently been extended to calculate the charge density of nuclei deformed at the mean-field level of approximation [J. M. Yao *et al.*, Phys. Rev. C **86**, 014310 (2012)]. The aim of this work is to further extend the method to the determination of transition densities between low-lying excited states.

Method: The starting point of our method is a set of Hartree-Fock-Bogoliubov wave functions generated with a constraint on the axial quadrupole moment and using a Skyrme energy density functional. Correlations beyond the mean field are introduced by projecting mean-field wave functions on angular momentum and particle number and by mixing the symmetry-restored wave functions.

Results: We give in this paper detailed formulas derived for the calculation of densities and form factors. These formulas are rather easy to obtain when both initial and final states are 0^+ states but are far from being trivial when one of the states has a finite J value. Illustrative applications to ^{24}Mg and to the even-mass $^{58-68}$Ni have permitted an analysis of the main features of our method, in particular the effect of deformation on densities and form factors. An illustrative calculation of both elastic and inelastic scattering form factors is presented.

Conclusions: We present a very general framework to calculate densities of and transition densities between low-lying states that can be applied to any nucleus. Achieving better agreement with the experimental data will require improving the energy density functionals that are currently used and also introducing quasiparticle excitations in the mean-field wave functions.

DOI: 10.1103/PhysRevC.91.024301　　PACS number(s): 21.10.Ft, 21.10.Ky, 21.60.Jz, 25.30.Bf

I. INTRODUCTION

Electron scattering off nuclei is a powerful tool for studies of nuclear structure and spectroscopy [1–16]. It allows determination of the charge distribution of nuclear ground states, as well as of the transition charge and current densities from the ground state to excited states. More global properties, such as charge radii, can be extracted from a detailed knowledge of charge distribution. Parameters characterizing the extension and surface thickness of the nuclear density can also be derived [17,18]. From the form factors for inelastic electron scattering at low transferred momentum q, the spin and parity of excited states and the multipole transition strengths can be determined in a model-independent manner [4,10]. At larger values of q, the form factors present an insight into the spatial location of the transition process, which cannot be accessed from the integral over this function provided by the measurement of $B(EL)$ values in Coulomb excitation or lifetime measurements. Thereby, electron scattering not only provides a powerful alternative to many other types of nuclear structure studies but also complements them by giving access to levels and transitions that are undetectable in photoexcitation and γ-ray spectroscopy, such as for instance levels excited by monopole transitions or transitions of high multipolarity.

As all electron-nucleus scattering experiments of the past used fixed or gas targets, only stable and a very few long-lived nuclides could be studied so far. This will change with the setup of electron-RIB collider experiments. The SCRIT (Self Confining Radioactive Isotope Target) project [19–21] is under construction at Rikagaku Kenkyusho (RIKEN) (Japan) and the ELISe (ELectron-Ion Scattering in a storage ring) project is planned for the GSI Facility for Antiproton and Ion Research (FAIR) (Germany) [22,23]. The charge densities and transition charge densities of short-lived nuclides, in particular neutron-rich nuclei, will be measured at both installations.

Data from electron scattering are often interpreted in terms of paramterized macroscopic density and transition density distributions, such as the ones of Helm [24], Tassie [25], or Friedrich *et al.* [17,18]. They all have in common that some functional form of the ground-state or transition charge densities is postulated and its parameters are adjusted to reproduce the data. Such analysis provides an insight into the gross features of the ground-state and transition charge density distribution and the resolution of their details [6]. For a more detailed analysis, however, it is desirable to calculate the form

---

[*] Present address: Department of Physics, Tohoku University, Sendai 980-8578, Japan.

factors from the same microscopic models that are also used to describe nuclear structure and spectroscopy. Most of them have been used to describe one and/or the other in the past.

(i) Shell-model calculations in small valence spaces have been used to calculate transition densities between states in light nuclei [26]. Some heavier nuclei have been calculated within the framework of the interacting Boson approximation [27]. In both cases, the truncation of the model space requires the introduction of effective charges and/or even explicitly calculated core polarization effects [26,28–31]. The no-core shell model, available only for light nuclei, is better suited in that respect [32,33].

(ii) Methods based on self-consistent mean fields [34] are a natural choice for such calculations, in particular for heavy nuclei, as they use a model space that comprises all occupied single-particle levels and an effective interaction or energy density functional (EDF) that is designed to reproduce nuclear saturation. Indeed, electron scattering form factors of spherical nuclei have already been studied in the pioneering papers of this field [35–38]. More recent studies emphasize the possible isospin dependence of the charge form factors of spherical nuclei [39–42]. With the exception of excitation to collective rotational states in well-deformed nuclei [43–46], pure mean-field calculations, however, are limited to ground-state densities. They also miss correlations from fluctuations in collective degrees of freedom and from symmetry restoration that should be considered for nonspherical nuclei.

(iii) The random phase approximation (RPA) (or the quasiparticle RPA) on top of mean-field calculations has been applied to spherical nuclei to study the ground-state and transition charge densities [47–55]. The extension of this framework to the density and transition density for deformed nuclei is, however, not trivial.

(iv) There also has been a number of studies where various electric and magnetic electron scattering form factors of deformed nuclei have been calculated by angular momentum projection of mean-field wave functions. To limit the computational cost, the wave functions were either restricted to be of a simple form [56] or the symmetry restoration was approximated in one way or the other [44,46,57–62]. For a presentation of the main aspects of these developments, see the review [63].

Recently, we have used the framework of the particle-number and angular-momentum-projected generator coordinate method (GCM) based on axial Hartree-Fock-Bogoliubov (HFB) states and a nonrelativistic Skyrme energy density functional to calculate the ground-state density of even-even nuclei [64], demonstrating how the correlations brought by going beyond a mean-field approach can quantitatively or even qualitatively alter the density profile predicted by pure mean-field methods. The same technique has been subsequently implemented in the relativistic framework using covariant energy density functionals [65–67]. Here, we extend the formalism of Ref. [64] to transition densities between low-lying excited states and the corresponding form factors as accessible by electron scattering. The emphasis of this first exploratory study is on the impact of static and dynamic quadrupole deformations on the transition density between low-lying collective states. Similar developments based on an angular-momentum and parity-projected GCM with (nonpaired) HF states, also using Skyrme interactions, have been recently reported in Ref. [68], but the calculations were limited to the simple case of elastic and inelastic transitions between 0^+ states.

The paper is organized as follows. In Sec. II we present the relevant formulas for the description of electron scattering off nuclei and the formalism for the calculations of nuclear density distribution and transition density for low-lying states in the framework of the projected GCM based on axially deformed HFB states. In Sec. III, we present an illustrative calculation of both elastic and inelastic scattering form factors for ^{24}Mg. Section IV details an application to the transition densities in even-mass $^{58-68}$Ni. The static and dynamic deformation effects on nuclear charge densities, transition charge densities, and form factors will be discussed in detail. Section V summarizes our findings, and four appendices provide further technical details on the calculation of nuclear form factors and the transition density.

II. FORMALISM

A. Beyond-mean-field description of nuclear states

Our beyond-mean-field method restores two of the symmetries relevant for nuclear spectroscopy that are broken by the self-consistent mean-field HFB method by projection on particle number and angular momentum. Fluctuations in shape degrees of freedom are described by the superposition of projected HFB states with different intrinsic deformations. The same formalism that is used to calculate operator matrix elements between projected states can be used to calculate projected densities and their form factors. Before entering into the details of their calculation, we first recall the main features of the method.

1. *Quadrupole deformed HFB states*

A set of deformed HFB states is generated by solving the HFB equations including a constraint on the axial quadrupole moment using an updated version of the code first described in [69]. The states are restricted to be time-reversal invariant and reflection symmetric, which implies that they are eigenstates of parity with eigenvalue +1. The HFB equations are complemented by the Lipkin-Nogami prescription to avoid the unphysical breakdown of pairing correlations at low density of single-particle levels around the Fermi energy.

The single-particle wave functions are discretized on a three-dimensional Cartesian coordinate-space mesh [70]. The step size of 0.8 fm ensures a good accuracy in the solution of the mean-field equations.

Throughout this study, we use the Skyrme parametrization SLy4 [71] together with a pairing energy functional of surface character [72] with parameters $\rho_0 = 0.16\ \mathrm{fm}^{-3}$ for the switching density and $V_0 = -1000\ \mathrm{MeV\,fm}^3$ for the pairing strength. A soft cutoff at ±5 MeV around the Fermi energy is used when solving the HFB equations as described in Ref. [72].

2. *Projected GCM states*

The GCM wave function [73] is constructed as a superposition of both particle-number and angular-momentum-projected HFB wave functions corresponding to different deformations $|q\rangle$,

$$|JM\mu\rangle = \sum_q F^J_{\mu,q}\,\hat{P}^J_{M0}\hat{P}^N\,\hat{P}^Z\,|q\rangle, \tag{1}$$

where μ labels different collective states for a given angular momentum J. This *ansatz* can cover a wide variety of situations, such as small fluctuations around a spherical or well-deformed minimum of a deep and steep potential well, wide fluctuations in soft nuclei, or mixing of states in different minima of the energy surface.

The operators $\hat{P}^Z$ and $\hat{P}^N$ project on proton and neutron number,

$$\hat{P}^N = \frac{1}{2\pi}\int_0^{2\pi} d\varphi\, e^{\mathrm{i}\varphi(\hat{N}-N)}, \tag{2}$$

and $\hat{P}^J_{MK}$ extracts eigenstates of total angular momentum J with z component M,

$$\hat{P}^J_{MK} = \frac{\hat{J}^2}{8\pi^2}\int d\Omega\,\mathcal{D}^{J*}_{MK}(\Omega)\,\hat{R}(\Omega), \tag{3}$$

where $\hat{J}^2 \equiv 2J+1$, $\hat{R}(\alpha,\beta,\gamma) \equiv e^{-i\alpha\hat{J}_x}\,e^{-i\beta\hat{J}_y}\,e^{-i\gamma\hat{J}_z}$ is the rotation operator, and $\mathcal{D}^J_{MK}(\alpha,\beta,\gamma)$ is the Wigner D function. Both the rotation operator and the Wigner D function depend on the Euler angles, for which we will use the shorthand notation $\Omega \equiv (\alpha,\beta,\gamma)$ whenever possible. The volume element of the integration over Euler angles is given by $d\Omega \equiv d\alpha\, d\beta\,\sin(\beta)\, d\gamma$. Only a $K=0$ component can be picked by $\hat{P}^J_{MK}$ from an HFB state that is axially symmetric around the z axis. Therefore, the index K will be dropped for simplicity.

The weight factors $F^J_{\mu,q}$ and the energies of the states $|JM\mu\rangle$ are obtained by solving a Hill-Wheeler-Griffin equation [73]

$$\sum_q \left(\mathcal{H}^J_{q'q} - E^J_\mu \mathcal{N}^J_{q'q}\right) F^J_{\mu,q} = 0, \tag{4}$$

for each value of J, where the norm kernel $\mathcal{N}^J_{q'q} = \langle q'|\hat{P}^J_{00}\hat{P}^N\,\hat{P}^Z|q\rangle$ and the energy kernel $\mathcal{H}^J_{q'q}$ is a functional of mixed densities [74]. More details about the calculations can be found in Ref. [75] and references given therein.

As the projected mean-field states do not form an orthogonal basis and the weights $F^J_{\mu,q}$ in Eq. (1) are not orthogonal functions, a set of orthonormal collective wave functions $g^J_{\mu,q}$ is constructed as [73]

$$g^J_{\mu,q} = \sum_{q'} (\mathcal{N}^J)^{1/2}_{qq'}\,F^J_{\mu,q'}, \tag{5}$$

but the modulus square of $g^J_{\mu,q}$ does not represent the probability of finding the deformation q in a GCM state $|JM\mu\rangle$. In a GCM based on axial states, however, the $g^J_{\mu,q}$ do nevertheless provide a good indication about the dominant configurations in the collective states $|JM\mu\rangle$.

B. Form factors in electron scattering

1. *General framework*

Our aim is to show how to calculate form factors and transition densities in the framework of our model. We will therefore not enter into the details of the process of scattering electrons off nuclei itself and limit the presentation to those elements of the formalism that are necessary to compute densities, transition densities, and their form factors in a form that can then be compared to experiment.

We use the framework of the plane-wave Born approximation (PWBA). The incident and outgoing electrons are described by plane waves $e^{i\mathbf{k}_i\cdot\mathbf{r}}$ and $e^{i\mathbf{k}_f\cdot\mathbf{r}}$ with momenta $\mathbf{k}_i$ and $\mathbf{k}_f$ and energies E^e_i and E^e_f, respectively. The differential cross section for electron scattering from a spinless nucleus is given by [2–4,7]

$$\frac{d\sigma}{d\Omega} = \frac{d\sigma_{\mathrm{M}}}{d\Omega}\sum_{L\geqslant 0}|F_L(q)|^2, \tag{6}$$

which is the product of the Mott cross section $d\sigma_{\mathrm{M}}/d\Omega$ describing the cross section for scattering off a pointlike target with charge Z [1,76] times the sum of form factors $F_L(q)$ that represent its modification by the nucleus having a finite size and an internal structure. The cross section depends on the momentum transfer $q = |\mathbf{k}_f - \mathbf{k}_i| \simeq 2\sqrt{E^e_i E^e_f}\,\sin(\theta/2)$, where $k_i(E^e_i)$ and $k_f(E^e_f)$ are the momenta (energies) of the incoming and outgoing electron, respectively, and θ the angle between $\mathbf{k}_i$ and $\mathbf{k}_f$.

The longitudinal Coulomb (CL) form factor $F_L(q)$ in (6) for an angular momentum transfer L is the Fourier-Bessel transform of the transition density $\rho^{J_f\mu_f}_{J_i\mu_i,L}(r)$ from an initial state $|J_i M_i \mu_i\rangle$ to a final nuclear state $|J_f M_f \mu_f\rangle$:

$$F_L(q) = \frac{\sqrt{4\pi}}{Z}\int_0^\infty dr\, r^2\,\rho^{J_f\mu_f}_{J_i\mu_i,L}(r)\,j_L(qr), \tag{7}$$

where the coefficient $\sqrt{4\pi}/Z$ is chosen so that the elastic part $(J_f = J_i, \mu_f = \mu_i)$ of the form factor $F_0(q)$ is unity at $q=0$. In this expression, $\rho^{J_f\mu_f}_{J_i\mu_i,L}(r)$ is the reduced transition density that will be related to GCM matrix elements in the next section.

In electron scattering off nuclei, the Coulomb attraction accelerates the electrons when they approach the nucleus and the electron wave is focused onto the nucleus. As a consequence, an experiment actually samples the form factor at a larger momentum transfer than given by the asymptotic values of the kinematic variables. This can be corrected for by plotting the experimental data measured for a given q [4,10,26] as a function of the corresponding "effective" momentum transfer

$$q_{\mathrm{eff}} = q\left(1 + \frac{3Ze^2}{2E^e_i R_{\mathrm{ch}}}\right), \tag{8}$$

where R_{ch} is the *equivalent hard-sphere radius* of the nucleus that is related to its rms charge radius r_{ch} by $R_{\mathrm{ch}} = \sqrt{5/3}\,r_{\mathrm{ch}}$.

Values for r_{ch} used in what follows are taken from a compilation of experimental data [77]. It was concluded in Ref. [26] that the Coulomb distortion effect of the scattered electrons is mostly taken into account by this prescription and that there is no significant advantage to replacing PWBA calculations for inelastic scattering with more involved distorted-wave Born approximation (DWBA) calculations, in particular when considering the limitations in precision of both data and their theoretical modeling.

A correction for the finite size of the proton is introduced by folding all calculated point proton densities with a Gaussian form factor [35], for example

$$\rho_{\mathrm{ch}}(\mathbf{r}) = \left(\frac{1}{a\sqrt{\pi}}\right)^3 \int d^3r'\ \exp\left[-\frac{(\mathbf{r}-\mathbf{r}')^2}{a^2}\right] \rho_p(\mathbf{r}'), \qquad (9)$$

where $a = \sqrt{2/3}\,\langle r^2\rangle_p^{1/2} = 0.65$ fm. When high precision is required, more detailed parametrizations of the proton and neutron charge distributions have to be used together with relativistic corrections (cf. [26,34] and references therein).

A correction for the spurious center-of-mass (c.m.) motion related to the breaking of translational invariance by the nuclear mean field should also be introduced. A rigorous way to remove it is to project on the c.m., which, however, is difficult to achieve in combination with angular-momentum projection for deformed states. As has been shown in such calculations for spherical mean-field states [78–80], the relative importance of the c.m. correction quickly fades away for heavy nuclei. A more economical approximation still in use [68] is the harmonic oscillator approximation first proposed in Ref. [81], where the calculated charge form factor is corrected by folding it with a c.m. motion correction $F_{\mathrm{ch,corr}}(q) = F_{\mathrm{ch}}(q)\,G_{\mathrm{cm}}(q)$ obtained in the harmonic oscillator approximation,

$$G_{\mathrm{cm}}(q) = \exp[q^2 b^2/(4A)], \qquad (10)$$

where $A = N + Z$ and b being a suitable oscillator length parameter [26]. In what follows, we will use $b = \sqrt{\hbar/m\omega_0}$, where m is the bare nucleon mass and the frequency ω_0 is given by $\hbar\omega_0 = 41\,A^{-1/3}$ MeV. As we will show below in Fig. 5, already for ^{24}Mg the effect of the c.m. motion correction is too small to be relevant for the purpose of our discussion.

2. Transition density between GCM states

To calculate form factors (7) for elastic and inelastic electron scattering and transition matrix elements, we need to determine the *reduced transition density* $\rho^{J_f\mu_f}_{J_i\mu_i,L}(r)$ as a function of the radial coordinate r. We now derive its relation to the *three-dimensional (3D) transition density* $\rho^{\alpha_f}_{\alpha_i}(\mathbf{r})$ between the initial $|\alpha_i\rangle$ and a final $|\alpha_f\rangle$ GCM states:

$$\begin{aligned}\rho^{\alpha_f}_{\alpha_i}(\mathbf{r}) &\equiv \langle\alpha_f|\hat\rho(\mathbf{r})|\alpha_i\rangle \\ &= \sum_{q'q} F^{J_f *}_{\mu_f,q'} F^{J_i}_{\mu_i,q}\,\rho^{\sigma_f q'}_{\sigma_i q}(\mathbf{r}),\end{aligned} \qquad (11)$$

where we have introduced the shorthand notation $\alpha \equiv \{JM\mu\}$ and $\sigma \equiv \{JMK\}$. With the exception of the appendices, we restrict the discussion to axial states and $\sigma \equiv \{JM0\}$. The density operator is defined as $\hat\rho(\mathbf{r}) \equiv \sum_i \delta(\mathbf{r}-\mathbf{r}_i)$, where $\mathbf{r}$ is the position at which the transition density is calculated, and $\mathbf{r}_i$ is the position of the ith nucleon.

The kernel of the *3D transition density* between two axial HFB states projected on particle numbers N,Z and angular momentum J is determined by

$$\rho^{\sigma_f q'}_{\sigma_i q}(\mathbf{r}) \equiv \langle q'|\hat P^{J_f}_{0M_f}\,\hat\rho(\mathbf{r})\,\hat P^{J_i}_{M_i0}\,\hat P^N\,\hat P^Z|q\rangle. \qquad (12)$$

The calculation of a matrix element like Eq. (12) can be simplified for an operator that is a spherical tensor by eliminating one of the two rotations [75,82,83]. The density operator, however, is not a spherical tensor operator; the evaluation of its matrix elements is considerably more complicated as both rotations in Eq. (12) will have to be carried out numerically.

Inserting the explicit expressions for the projection operators into Eq. (12), one obtains for the transition density kernel (see Appendix B for further details)

$$\begin{aligned}\rho^{\sigma_f q'}_{\sigma_i q}(\mathbf{r}) = \frac{\hat J_f^2}{8\pi^2}\int d\Omega'\ D^{J_f}_{M_f0}(\Omega') \\ \times \sum_K D^{J_i *}_{M_iK}(\Omega')\,\hat R(\Omega')\,\rho^{J_iK0}_{q'q}(\mathbf{r}),\end{aligned} \qquad (13)$$

where $\rho^{J_iK0}_{q'q}(\mathbf{r})$ for axially deformed nuclei is simplified as

$$\begin{aligned}\rho^{J_iK0}_{q'q}(\mathbf{r}) \equiv \frac{\hat J_i^2}{2}\int_0^\pi d\beta\ \sin(\beta)\,d^{J_i}_{K0}(\beta) \\ \times \langle q'|\hat\rho(\mathbf{r})\,\hat P^N\,\hat P^Z\,\hat R_y(\beta)|q\rangle.\end{aligned} \qquad (14)$$

The calculation of the density (14) requires the determination of nondiagonal matrix elements of the density operator between a rotated and a nonrotated state analogous to the calculation of projected matrix elements of tensor operators [75,82,83]. As shown in Ref. [82], when the x signature is preserved, the integrant $\rho_{q'q}(\mathbf{r},\beta) \equiv \langle q'|\hat\rho(\mathbf{r})\,\hat P^N\,\hat P^Z\,\hat R_y(\beta)|q\rangle$ presents a symmetry in β with respect to $\pi/2$:

$$\rho_{q'q}(x,y,z,\pi-\beta) = \rho_{q'q}(-x,y,z,\beta), \qquad (15)$$

which can be used to reduce the number of density overlaps to be calculated explicitly by a factor of 2.

Compared to the calculation of operator matrix elements, the unfamiliar element in the calculation of the projected transition density kernels (13) is that the integration over Ω' cannot be carried out analytically. Instead, Eq. (13) involves the rotation of the density $\rho^{J_iK0}_{q'q}(\mathbf{r})$ as a whole.

In a 3D coordinate-space representation as used here, a rotation requires an interpolation of the rotated function, as the rotated coordinates of the mesh points do in general not fall back on the mesh. In our case, the integration over $d\cos(\beta)$ is discretized using a Gauss-Legendre quadrature with 24 points in the interval $[-1,+1]$, which is sufficient for the low values of J considered here. The corresponding rotations $\hat R_y(\beta)$ in (14) are carried out with the same accurate Lagrange-mesh technique [84,85] that is also used to evaluate operator matrix elements in our codes.

To perform the rotation of $\rho^{J_iK0}_{q'q}(\mathbf{r})$ in Eq. (13), it turned out that, instead of a rotation of the density followed by an integration over Euler angles, it is advantageous to expand

$\rho_{q'q}^{J_i K 0}(\mathbf{r})$ into spherical harmonics first. Using the transformation of spherical harmonics under rotation and some further angular-momentum algebra that is detailed in Appendix C, the integrals over Euler angles Ω' in Eq. (13) can be transformed into integrals over spatial angles that are much easier to carry out:

$$\rho_{\sigma_i q}^{\sigma_f q'}(\mathbf{r}) = \frac{\hat{J}_f^2}{\hat{J}_i^2} \sum_{K\lambda\nu'} \langle J_f 0 \lambda K | J_i K\rangle \, \langle J_f M_f \lambda \nu' | J_i M_i\rangle \times \rho_{q'q;\lambda K}^{J_i K 0}(r) \, Y_{\lambda\nu'}(\hat{\mathbf{r}}), \quad (16)$$

where $\rho_{q'q;\lambda K}^{J_i K 0}(r)$ is given by

$$\rho_{q'q;\lambda K}^{JK0}(r) = \int d\hat{\mathbf{r}}' \, \rho_{q'q}^{J_i K0}(r,\hat{\mathbf{r}}') \, Y^*_{\lambda K}(\hat{\mathbf{r}}'). \quad (17)$$

Finally, the 3D transition density of an axially deformed nucleus is given by

$$\rho_{\alpha_i}^{\alpha_f}(\mathbf{r}) = \frac{\hat{J}_f^2}{\hat{J}_i^2} \sum_{K\lambda\nu'} \langle J_f 0 \lambda K | J_i K\rangle \langle J_f M_f \lambda \nu' | J_i M_i\rangle \times Y_{\lambda\nu'}(\hat{\mathbf{r}}) \int d\hat{\mathbf{r}}' \rho_{\mu_f\mu_i}^{J_f J_i K 0}(r,\hat{\mathbf{r}}') Y^*_{\lambda K}(\hat{\mathbf{r}}'), \quad (18)$$

where we have introduced a configuration-mixing *pseudo GCM density*[1]

$$\rho_{\mu_f\mu_i}^{J_f J_i K 0}(\mathbf{r}) \equiv \sum_{q'q} F_{\mu_f,q'}^{J_f 0*} \, F_{\mu_i,q}^{J_i 0} \, \rho_{q'q}^{J_i K0}(\mathbf{r}). \quad (19)$$

After some further algebraic manipulations, one obtains the expression of the radial part of the 3D transition density, namely, the *reduced transition density* [cf. (C9)]

$$\rho_{J_i\mu_i,L}^{J_f\mu_f}(r) = (-1)^{J_i - J_f} \frac{\hat{J}_f^2}{\hat{J}_i^2} \sum_K \langle J_f 0 L K | J_i K\rangle \times \int d\hat{\mathbf{r}} \, \rho_{\mu_f\mu_i}^{J_f J_i K 0}(\mathbf{r}) \, Y^*_{LK}(\hat{\mathbf{r}}) \quad (20)$$

that is experimentally accessible via electron scattering.

Compared to the direct evaluation of Eq. (13), the expansion in spherical harmonics has the practical advantage in separating the radial dependence of $\rho_{J_i\mu_i,L}^{J_f,\mu_f}(\mathbf{r})$, which is specific to each state, from its angular dependence, which is completely determined by the angular momentum quantum numbers of the states.

The integration over the angular part of $\mathbf{r}$ in Eq. (20) is discretized using a Gauss-Legendre quadrature with 20 points for the cosine of the polar angle $\cos(\theta)$ and a trapezoidal rule with 20 points for the azimuthal angle φ. To carry out the integral, the density $\rho_{q'q}^{J_i K 0}(\mathbf{r})$ that is calculated on a equidistant Cartesian mesh has to be interpolated to the mesh points in spherical coordinates by using the Lagrange-mesh interpolation [84]. The step size dx of the original Cartesian mesh is kept for the radial coordinate r.

3. *Transition densities in some special cases*

The expression for the inelastic scattering transition density (TD), given by Eq. (18), simplifies greatly if the initial state is a 0^+ state:

$$\rho_{0^+_{\mu_i}}^{\alpha_f}(\mathbf{r}) = Y^*_{J_f M_f}(\hat{\mathbf{r}}) \int d\hat{\mathbf{r}}' \; \rho_{\mu_f\mu_i}^{J_f 000}(r,\hat{\mathbf{r}}') \, Y_{J_f 0}(\hat{\mathbf{r}}'). \quad (21)$$

As expected, the angular part of this TD is given by $Y^*_{J_f M_f}(\hat{\mathbf{r}})$. The reduced transition density becomes

$$\rho_{0\mu_i,L}^{J_f\mu_f}(r) = \hat{J}_f \int d\hat{\mathbf{r}} \; \rho_{\mu_f\mu_i}^{J_f 000}(\mathbf{r}) \, Y_{J_f 0}(\hat{\mathbf{r}}) \, \delta_{J_f L}. \quad (22)$$

For a well-deformed nucleus, which can be described by a single axial HFB configuration $|q_0\rangle$, and by assuming that the overlap between the rotated wave function and the original one can be approximated by a $\delta(\Omega)$ function, the pseudo GCM density $\rho_{\mu_f\mu_i}^{J_f J_i K 0}(\mathbf{r})$ reduces to the intrinsic density, projected on particle numbers, $\rho_{q_0 q_0}^{NZ}(\mathbf{r}) \equiv \langle q_0 | \hat{\rho}(\mathbf{r}) \, \hat{P}^N \, \hat{P}^Z | q_0\rangle$. The transition density $\rho_{01,L}^{L\mu_f}(r)$ in Eq. (20) is then simply given by

$$\rho_{01,L}^{L\mu_f}(r) = \hat{L} \int d\hat{\mathbf{r}} \; \rho_{q_0 q_0}^{NZ}(\mathbf{r}) \, Y_{L0}(\hat{\mathbf{r}}), \quad (23)$$

showing that we recover the rigid-rotor model for well-deformed nuclei. The quality of this approximation quickly deteriorates with increasing L values, as illustrated in Refs. [10,57].

By putting $\alpha_i = \alpha_f = \alpha$ in Eq. (18), the 3D density for the GCM state $|\alpha\rangle$ is given by

$$\rho_\alpha^\alpha(\mathbf{r}) = \sum_\lambda Y_{\lambda 0}(\hat{\mathbf{r}}) \, \langle J M \lambda 0 | J M\rangle \sum_K \langle J 0 \lambda K | J K\rangle \times \int d\hat{\mathbf{r}}' \; \rho_{\alpha\alpha}^{JJK0}(r,\hat{\mathbf{r}}') \, Y^*_{\lambda K}(\hat{\mathbf{r}}'). \quad (24)$$

For the ground state 0_1^+, it is just the average of the pseudo GCM density $\rho_{11}^{0000}(r,\hat{\mathbf{r}}')$ over the angular coordinates,

$$\rho_{0_1^+}^{0_1^+}(\mathbf{r}) = \frac{Y_{00}(\hat{\mathbf{r}})}{\sqrt{4\pi}} \int d\hat{\mathbf{r}}' \; \rho_{11}^{0000}(r,\hat{\mathbf{r}}'), \quad (25)$$

which obviously is spherically symmetric. This density has been recently determined for various light systems using the symmetry-restored GCM method [64–66].

4. *Multipole transition matrix elements*

The multipole transition matrix elements that are frequently calculated in angular-momentum-projected GCM calculations are related to the transition density (20) through

$$M_{J_i\mu_i,L}^{J_f\mu_f} = \int_0^\infty dr \, r^{L+2} \, \rho_{J_i\mu_i,L}^{J_f\mu_f}(r) = \hat{J}_i^{-1} \sum_{q'q} F_{\mu_f,q_f}^{J_f *} F_{\mu_i,q_i}^{J_i} \langle J_f q' || \hat{Q}_L || J_i q\rangle, \quad (26)$$

---

[1] This *pseudo GCM density* summarizes all the information related to the GCM calculation but it is not an observable.

where the reduced matrix element of the multipole operator $\hat{Q}_{LM}(\mathbf{r}) \equiv r^L Y_{LM}(\hat{\mathbf{r}})$ is defined by

$$\begin{aligned}\langle J_f q' || \hat{Q}_L(\mathbf{r}) || J_i q \rangle \equiv{}& \frac{\hat{J}_f^2 \hat{J}_i^2}{2} (-1)^{J_f} \sum_M \begin{pmatrix} J_f & L & J_i \\ 0 & M & -M \end{pmatrix} \\ &\times \int_0^\pi d\beta \, \sin(\beta) \, d^{J_i *}_{-M0}(\beta) \\ &\times \langle q' | r^L Y_{LM}(\hat{\mathbf{r}}) \, \hat{P}_N \hat{P}_Z \hat{R}_y(\beta) | q \rangle . \end{aligned} \tag{27}$$

The electric multipole transition strengths $B(EL : \alpha_i \to \alpha_f)$ are then given by the square of the proton part of the transition matrix element $M^{J_f \mu_f}_{J_i \mu_i, L}$ (abbreviated with M^p_L). More details are given in Appendix D.

There have been efforts to deduce the multipole transition matrix elements M^p_L and M^n_L of protons and neutrons by combining Coulomb excitation and (p,p') measurements [86], which, however, requires model assumptions at several stages of the analysis. While their experimental determination remains debatable, it turns out that the comparison between the calculated M^p_L and M^n_L sheds light on the relative contributions by the neutrons and protons to the nuclear excitation, and therefore it provides an insight into the isospin nature of the *calculated* excitation modes. The deviation of a factor η defined as

$$\eta = \frac{M^n_L / M^p_L}{N/Z} \tag{28}$$

from 1.0 is then interpreted as the measure of the isovector character of the excitation [86]. This quantity provides a tool to study the isospin nature of the excitations, as the multipole moments of neutrons can be easily calculated in the same way as the ones of protons.

III. ILLUSTRATIVE APPLICATION TO ^{24}Mg

The nucleus ^{24}Mg has been used as a testing ground for many implementations of beyond-mean-field models [75,82,83,85,87,88]. The results presented here are an extension of previous studies. The mass quadrupole moment is discretized with a step size $\Delta q = 40$ fm^2, ranging from -200 to $+360$ fm^2. This choice ensures good convergence of the GCM calculation. The excitation spectra obtained here are the same as those reported for axial calculations in Ref. [75].

The energy curves obtained after projection on particle numbers only and after simultaneous projections on particle numbers and angular momentum $J = 0, 2$, and 4 are plotted in Fig. 1(a). They are drawn as a function of the scaled quadrupole moment β_2 defined as

$$\beta_2 = \sqrt{\frac{5}{16\pi}} \frac{4\pi}{3R^2 A} \langle q | 2\hat{z}^2 - \hat{x}^2 - \hat{y}^2 | q \rangle , \tag{29}$$

where $R = 1.2 A^{1/3}$ fm and varies from -0.9 to $+1.6$. The energies of the first GCM states are also indicated by dots centered at their mean deformations $\bar{\beta}_{J\mu}$ defined as

$$\bar{\beta}_{J\mu} = \sum_q \beta_2(q) \, |g^J_{\mu,q}|^2 . \tag{30}$$

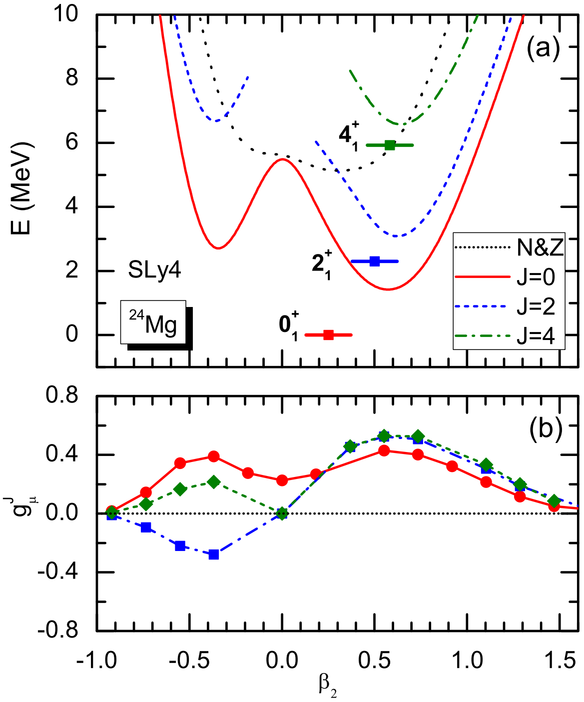

FIG. 1. (Color online) (a) Total energy (normalized to the 0^+_1 state) for the particle-number-projected HFB states (N&Z) and for the particle-number and angular-momentum-projected states (curves for $J = 0$, 2, and 4) for ^{24}Mg as a function of the intrinsic mass quadrupole deformation of the mean-field states. The solid squares indicate the lowest GCM solutions, which are plotted at their average deformation $\bar{\beta}_{J\mu}$. (b) Collective wave functions $g^J_{\mu,q}$ [cf. Eq. (5)] of the 0^+_1, 2^+_1, and 4^+_1 states.

Although $\bar{\beta}_{J\mu}$ is not an observable, in axial calculations it often provides a good indication about the dominant mean-field configurations in a GCM state.

The corresponding collective wave functions are shown in Fig. 1(b). The 0^+_1, 2^+_1, and 4^+_1 states are a mixing of projected prolate and oblate deformed configurations, with a dominance of the prolate ones.

Contour plots of the proton densities $\rho^\alpha_\alpha(\mathbf{r})$, Eq. (24), in the $y = 0$ plane are shown in Fig. 2 for the $M = 0$ orientation of the $J^\pi = 0^+$, 2^+_1, and 4^+_1 states. As expected, the density of the 0^+_1 state is spherical after projection, The densities

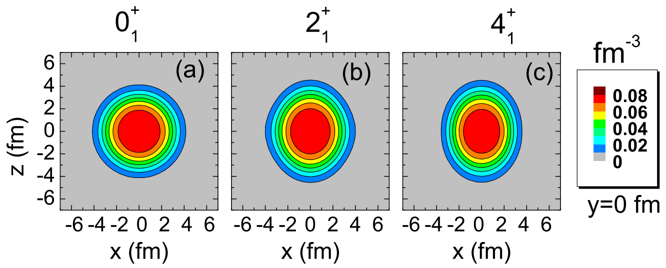

FIG. 2. (Color online) Contour plots of calculated 3D proton densities $\rho^\alpha_\alpha(\mathbf{r})$ (in fm^{-3}) in the $y = 0$ plane for the 0^+_1 (a), 2^+_1 (b), and 4^+_1 (c) states (with $M = 0$) in ^{24}Mg.

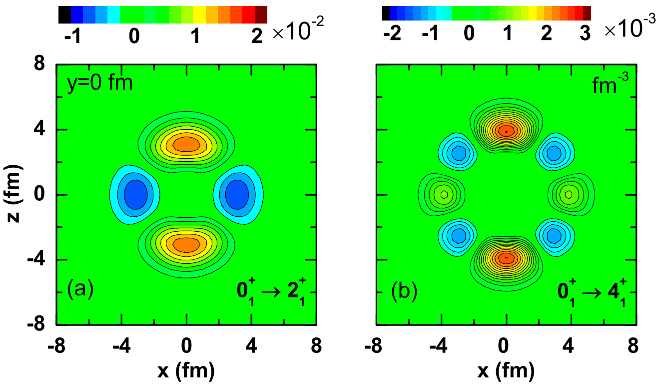

FIG. 3. (Color online) Contour plots of calculated TPD $\rho^{\alpha_f}_{0_1^+}(\mathbf{r})$, Eq. (21), in fm^{-3} in the $y=0$ plane for the inelastic scattering from the ground state to the 2_1^+ (a) and the 4_1^+ (b) states with $M=0$ in ^{24}Mg.

of the 2_1^+ and 4_1^+ states are a superposition of spherical harmonics with λ values ranging from 0 to $2J$ [see Eq. (24)]. Their elongation along the z axis is larger than along the x and y axes, giving the shapes a prolate-like form. The dimensionless quadrupole deformations $\beta^{(s)}$ determined from the spectroscopic quadrupole moments $Q_s(J_\mu)$ of $K=0$ states,

$$\beta^{(s)}(J_k)=\sqrt{\frac{5}{16\pi}}\frac{4\pi}{3ZR^2}\left(-\frac{2J+3}{J}\right)Q_s(J_\mu), \tag{31}$$

are $\beta^{(s)}=0.55$ for the 2_1^+ and 0.63 for the 4_1^+ states, respectively. The spectroscopic quadrupole moment $Q_s(J_\mu)$ is given by the expectation value of the quadrupole operator $\hat{Q}_{20}(\mathbf{r})=r^2\,Y_{20}(\hat{\mathbf{r}})$, multiplied by a coefficient $\sqrt{16\pi/5}$:

$$Q_s(J_\mu)=\sqrt{\frac{16\pi}{5}}\langle J\,J20|J\,J\rangle\,M^{J\mu}_{J\mu,2}, \tag{32}$$

with $M^{J\mu}_{J\mu,2}$ as defined in Eq. (26).

Figure 3 displays the transition proton density (TPD) $\rho^{\alpha_f}_{0_1^+}(\mathbf{r})$ [cf. Eq. (21)] for the inelastic scattering from the ground state to the 2_1^+ and 4_1^+ states of ^{24}Mg. The density for the transition from the 0_1^+ ground state to the 4_1^+ state is an order of magnitude smaller than the one to the 2_1^+ state. As expected from Eq. (21), the angular part of the TPDs has the shape of a spherical harmonic. They are the largest around the nuclear surface and present lobes of alternating signs.

The elastic C0 form factor $|F_0(q)|^2$ for the ground state of ^{24}Mg is plotted in Fig. 4. The GCM calculation reproduces the position of the form factor minima and is in agreement with the data at low q values. However, our result underestimates largely the form factor after the first minimum. A similar discrepancy was found in Ref. [68] in the case of ^{12}C. There, it has been argued that the spreading of the collective wave function on many deformations creates a too large smoothing of the one-body density and decreases the weights of the large-q components of the transition density. In the case of ^{12}C, the pure HF form factor was slightly in better agreement with the data. To estimate the effect of deformation on the form factors, we also show the results obtained from single-configuration calculations based on either $\beta_2=0$ (spherical shape) or $\beta_2=0.55$ (minimum of the $J=0$ energy curve) wave functions. The form factor corresponding to the projection of the deformed configuration differs only marginally from the GCM result. A similar result has also been found for ^{46}Ar in Ref. [66]. On the contrary, the high-q components of the form factor based on the spherical configuration are much larger and in better agreement with the data. As can be seen from the inset, the charge density of the spherical configuration is also larger in the interior than the densities obtained from $J=0$ projected deformed configurations. Since it is well established that ^{24}Mg is deformed, the discrepancy between the GCM result and experiment at large q values points toward missing components in the ground-state wave function.

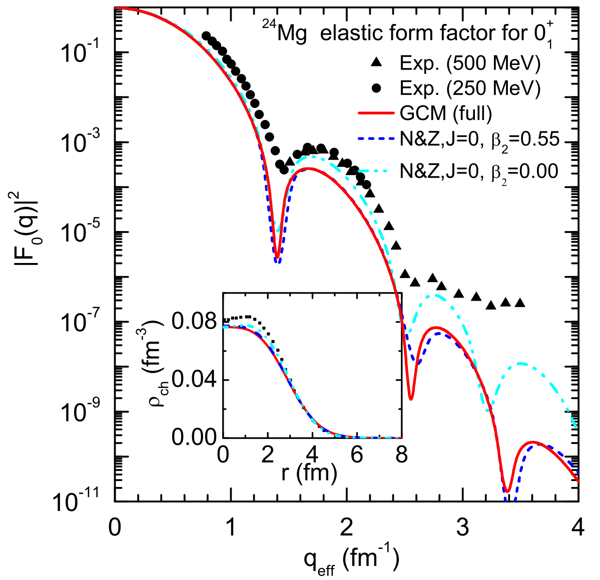

FIG. 4. (Color online) Elastic C0 form factor $|F_0(q)|^2$ for the 0_1^+ ground state of ^{24}Mg, in comparison with several calculations: he C0 form factor obtained by particle-number and $J=0$ projection of a single HFB state with either $\beta_2=0$ (spherical shape; light blue dash-dotted curve) or $\beta_2=0.55$ (minimum of $J=0$ projected energy curve; dark blue dashed curve) and from the full projected GCM calculation (red solid curve). The inset shows the corresponding charge density. Data (solid triangles and circles) are taken from Ref. [89].

In Refs. [17,18], Friedrich and collaborators have performed a detailed analysis of the relation between various parametric forms of charge density distributions and the resulting form factors. They conclude that the first zero of $|F_0(q)|^2$ determines an extension parameter of the charge distribution. Indeed, their analysis shows that, when comparing two different C0 form factors, a minimum at lower q values corresponds to a larger extension of the nuclear density. By contrast, the surface diffuseness of the charge distribution is related to the height of the first maximum of $|F_0(q)|^2$. For each of the three calculations shown in Fig. 4, the first minimum of $|F_0(q)|^2$ is located at nearly the same value of q, indicating similar extensions. The value of $|F_0(q)|^2$ at the first maximum, however, is significantly larger for the spherical configuration

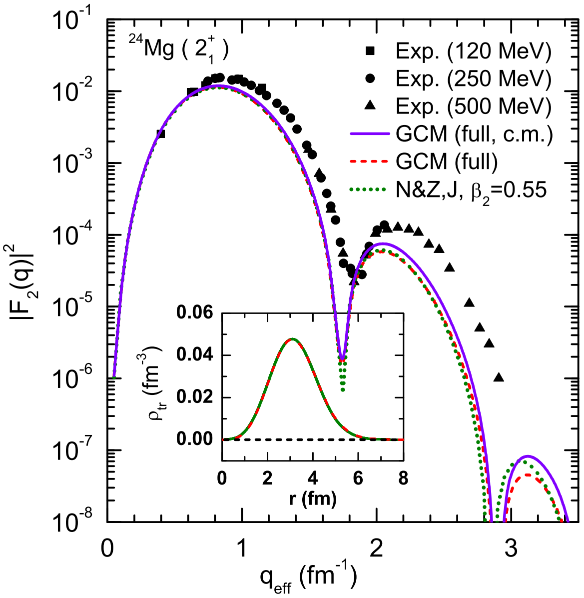

FIG. 5. (Color online) Longitudinal C2 form factor $|F_2(q)|^2$ for the transition from the ground state to the 2^+_1 state for ^{24}Mg, in comparison with available data. The form factor calculated with only one single configuration of $\beta_2 = 0.55$ and the form factor of the transition proton density from full GCM calculations are given for comparison. The inset shows the corresponding transition densities. Data are taken from Ref. [90] (squares) and Ref. [89] (circles and triangles).

and corresponds to a lower surface thickness, as can be seen on the plot of the density.

The C2 longitudinal inelastic form factor is plotted in Fig. 5 for the transition from the ground state to the 2^+_1 state in ^{24}Mg. Results obtained by projecting a single deformed HFB state with $\beta_2 = 0.55$ on $J = 0$ and $J = 2$ are compared with the full projected GCM calculation and with experimental data. The spreading of the GCM wave function over deformation has little effect. As for $|F_0(q)|^2$, the GCM $|F_2(q)|^2$ form factor is too low at large q values. A possible cause for this deficiency could be a lack of components not included in the mean-field basis. However, since we are using effective interactions, a shortfall of the EDF cannot be excluded either. To estimate the spurious effect of the c.m. motion, we have introduced a correction in the form given by Eq. (10). Although this correction is too small, it is going in the right direction.

Figure 6 displays the q-dependent transition quadrupole matrix element $M_2(q^2)$, Eq. (A15), for the transition from the ground state to the 2^+_1 state. The calculated values agree well with the available data. According to Eqs. (A13) and (A15), the transition strength $B(E2)$ is given by the square of $M_2(q^2)$ in the $q \to 0$ limit. The $B(E2\uparrow)$ value determined in this way from the inelastic scattering data in low-q region is 420 ± 25 e^2 fm^4 [90], which is slightly overestimated by our calculation, which gives a value of about 450 e^2 fm^4.

Figure 7 displays the C4 longitudinal inelastic form factor $|F_4(q)|^2$ from the ground state to the 4^+_1 state. The experimental data are taken from Ref. [91]. The calculation reproduces well the diffraction minimum observed at $q \simeq 2.0$ fm^{-1} in the data.

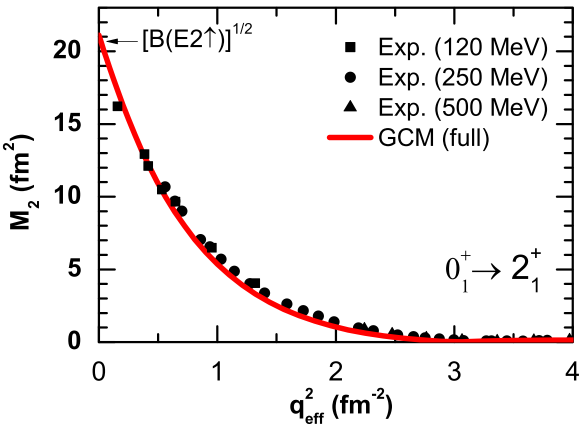

FIG. 6. (Color online) q-dependent transition quadrupole matrix element $M_2(q^2)$, Eq. (A15), for the $E2$ transition from the ground state to the 2^+_1 state in ^{24}Mg, in comparison with available data. $M_2(q^2)$ in the $q \to 0$ limit is related to the $B(E2)$ value via $M_2(0) = \sqrt{B(E2)}/e$. Data are taken from Ref. [90] (squares) and Ref. [89] (circles and triangles).

Moreover, the calculated $E4$ transition strength $B(E4 : 0^+_1 \to 4^+_1) = 2.07 \times 10^3$ e^2 fm^8 is close to the experimental value of $2.0(3) \times 10^3$ e^2 fm^8 [91]. The $L = 4$ transition density, shown in the inset of Fig. 7, is peaked at $r \simeq 4.0$ fm, further out than the $L = 2$ transition density that has been shown in Fig. 5.

IV. APPLICATION TO EVEN-MASS $^{58-68}$Ni

The stable Ni isotopes ($A = 58$ to 62) have been extensively studied in the 1960s. The data have been extended to heavier isotopes over the past ten years, going up to potentially neutron magic numbers $N = 40$ and $N = 50$. There is now a large set of data putting into evidence the complexity of the evolution of the Ni shell structure with the number of neutrons (see for instance the discussions in Refs. [92–94]).

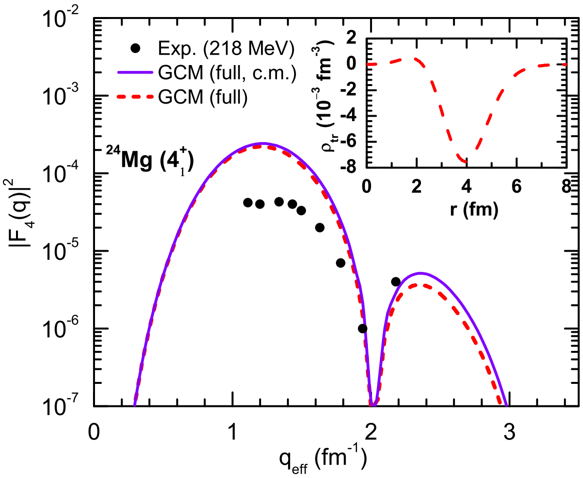

FIG. 7. (Color online) Longitudinal C4 form factor $|F_4(q)|^2$ for the transition from the ground state to the 4^+_1 state of ^{24}Mg, in comparison with available data. The inset shows the corresponding transition density. Data are taken from Ref. [91].

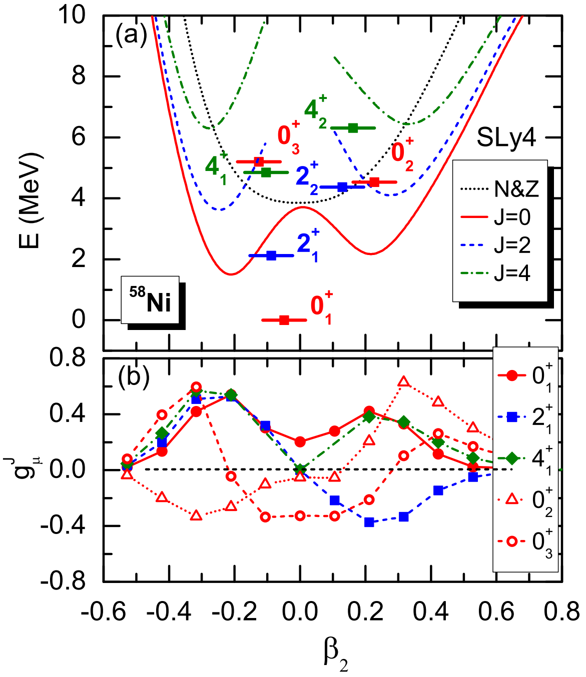

FIG. 8. (Color online) Same as Fig. 1, but for ^{58}Ni.

The discretization of the mass quadrupole moment used for the GCM calculations of the Ni isotopes ranges from -500 to $+700$ fm^2 with a step size $\Delta q = 100$ fm^2.

The results obtained at the successive steps of our method for ^{58}Ni are plotted in Fig. 8. The energy curve obtained from particle-number projection of mean-field wave functions presents a soft spherical minimum. After projection on angular momentum, two minima, close in energy, are obtained for $J = 0$, 2, and 4 by the projection of prolate and oblate mean-field configurations. The collective wave functions g^J_μ resulting from configuration mixing are spread over a large range of deformations [see Fig. 8(b)]. As a consequence, the mean deformation $\bar{\beta}_{J\mu}$ is close to zero and does not bring valuable information. By contrast, the positive $\bar{\beta}_{J\mu}$ of the first excited states indicates that they are dominated by prolate mean-field configurations.

There have been claims in the literature that ^{58}Ni is a spherical vibrator (see for instance Refs. [95,96]). The calculated energy pattern that we obtain, shown in Fig. 9, has indeed some of the characteristics expected for a vibrator [97]. The first 4^+ and second 2^+ levels are at about twice the energy of the 2^+_1 state. There are, however, two near-degenerate 0^+ levels at the expected energy of the two-phonon state instead of just one. Looking at transition probabilities, one sees that the first excited 0^+ has a strong deexcitation to the second 2^+ state, which is incompatible with a simple vibrator. The second excited 0^+ decays predominantly to the first 2^+ and would thus be a better candidate for a two-phonon state, but the overall pattern of $B(E2)$ values is very different from what would be expected. The available data for ^{58}Ni are too sparse to draw firm conclusions, but they do not seem to be well described by the assumption of a simple vibrator either. In fact, there seems to be a general rule that the more information about a potential anharmonic vibrator becomes available, the less this interpretation can be retained [97,98].

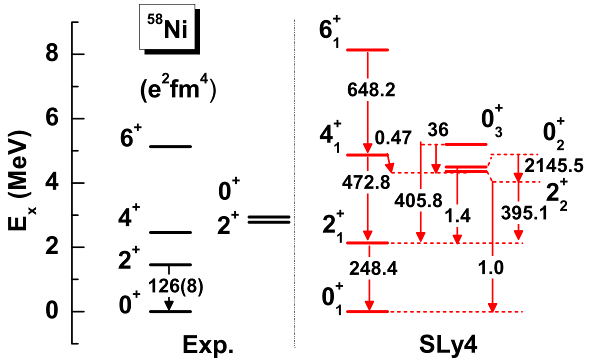

FIG. 9. (Color online) Comparison between the spectrum obtained for ^{58}Ni using our method and the experimental results. Data are taken from Ref. [94].

The shell-model description of this Ni isotope, and also of all others up to ^{68}Ni, shows that a correct reproduction of both energies and $B(E2)$ values of the low-lying states requires the inclusion of the full fp shell (see the discussion in Ref. [93]). In its present form, our beyond-mean-field method does not allow us to include all the relevant shell-model configurations: Multiple quasiparticle excitations that break time-reversal invariance are not contained in the model space used in this study. However, deformed configurations include many spherical multiparticle-multihole excitations. The spreading of the GCM wave functions over a large range of deformations is an economic way to include spherical orbitals arising from shells excited at sphericity (see Fig. 13).

The elastic scattering form factor for ^{58}Ni is shown in Fig. 10. The results obtained with the full GCM basis are compared to those corresponding to the projection of a single configuration, either spherical or corresponding to the minima at $\beta_2 = \pm 0.21$ of the projected energy curve. All these form factors are quite close, with slight differences at q values beyond the first maximum. The position of the zeros is reproduced rather well, but the heights of the first and second diffraction maxima are underestimated.

The ground-state charge density distribution is plotted in Fig. 11 for the same four calculations as in Fig. 10. The small differences between these calculations above $q = 1.2$ fm^{-1} is reflected in differences between the densities in the interior region ($r < 2.0$ fm). The GCM result is similar to a previous result obtained from a one-dimensional Bohr Hamiltonian (1DBH) calculation determined by the HFB method and using the Gogny D1 force [101].

To analyze the effect of static deformations, we compare in Fig. 12 the elastic form factor and the charge distribution calculated using projected deformed configurations with increasing values of β_2 from spherical to $\beta_2 = 0.7$. The height of the first and second diffraction maxima is not affected by small deformations. However, it starts to significantly decrease with deformation for β_2 values larger than 0.2. Moreover, the C0 form factor drops faster in the low-q region if the deformation is increased, as shown in the inset of Fig. 12. This behavior can be understood by looking to the relation (A16) between

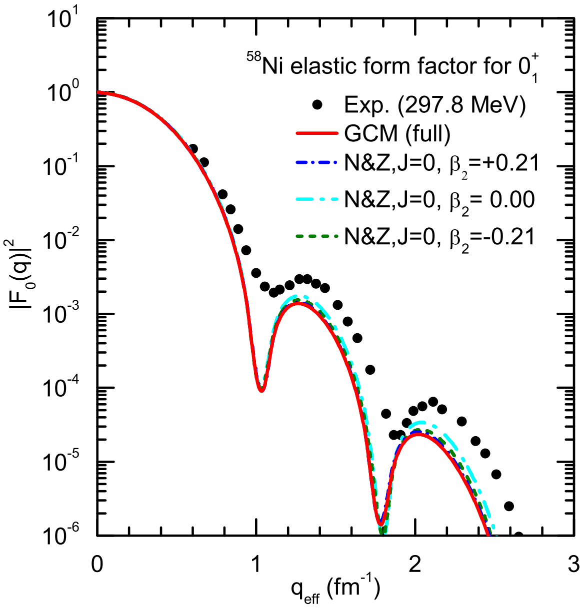

FIG. 10. (Color online) Data for the elastic form factor $|F_0(q)|^2$ for the ground state of ^{58}Ni taken from Ref. [99] in comparison with the form factor obtained from four different calculations: projection of a single HFB configuration with either $\beta_2 = 0$ (spherical shape) or $\beta_2 = \mp 0.21$ (oblate and prolate minima of the $J = 0$ energy curve) and full GCM of projected states.

the C0 form factor and the rms charge radii $r_{\rm ch}$ for low-q values and from the effect of deformation on the charge radius of a uniformly charged liquid drop, $r_{\rm ch}/r_{\rm ch}^{\rm sph} \simeq (1 + \frac{5}{4\pi}\,\beta_2^2)$. Figure 12(b) illustrates the effect of deformation on the charge density distribution. Increasing the deformation pushes charge from the inside of the surface (around $r = 3$ fm) to the outside (around $r = 6$ fm).

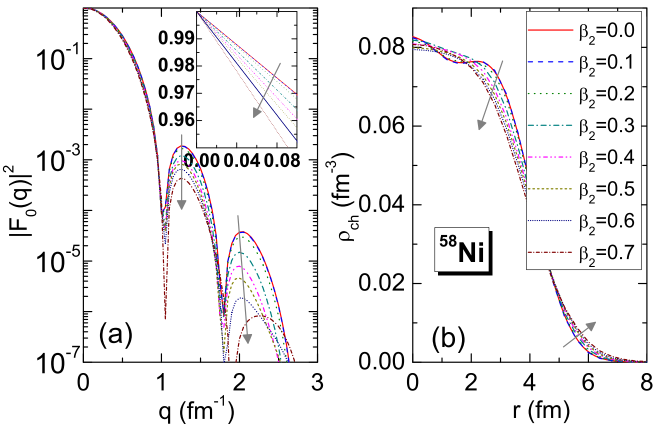

FIG. 12. (Color online) (a) Elastic form factor $|F_0(q)|^2$ for the $J = 0$ state of ^{58}Ni projected from a single HFB configuration with prolate deformation of β_2 increasing from 0.0 to 0.7, respectively. (b) Charge distributions corresponding to the form factors displayed in panel (a).

The origin of the change of behavior of $|F_0(q)|^2$ at $\beta_2 \approx 0.3$ can be traced back to the single-particle spectra. These are plotted in Fig. 13. The shell structure for neutrons and for protons is very similar. At $\beta_2 \approx 0.3$, a downsloping proton level from the $1f_{7/2}$ spherical shell crosses an upsloping level from the $2p_{3/2}$ shell. This indicates that the gradual population of the $2p_{3/2}$ orbital beyond this point might be responsible for the decrease of the form factor at large q values.

In the next figures, we show results obtained for the even Ni isotopes up to $N = 40$. Figure 14 shows the evolution with

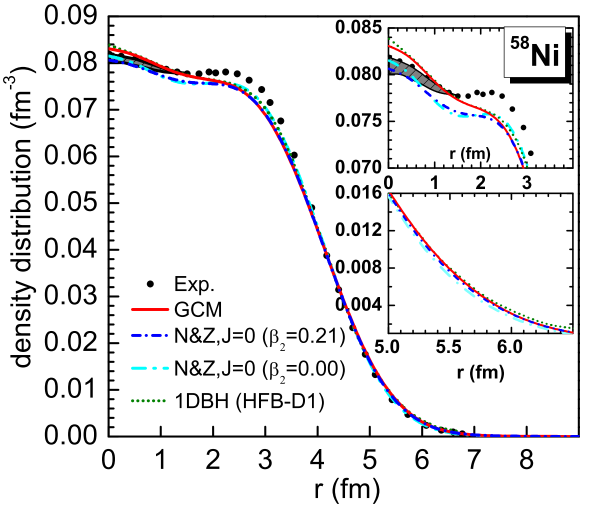

FIG. 11. (Color online) Comparison between the charge distribution of the ground state of ^{58}Ni obtained using single projected mean-field configurations or the full GCM basis and the experimental data [100]. A previous calculation using a one-dimensional Bohr Hamiltonian based on an HFB calculation with the Gogny D1 force (1DBH) [101] is also shown. The insets magnify the profile of the charge density at very small radii and in the nuclear surface.

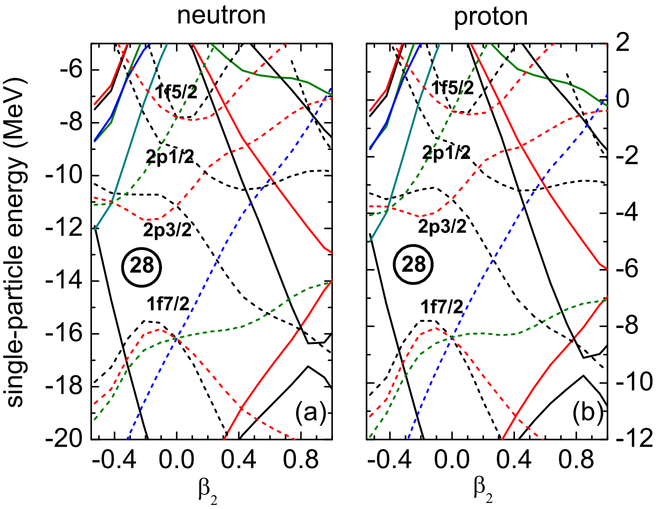

FIG. 13. (Color online) Nilsson diagram of the eigenvalues of the single-particle Hamiltonian for neutrons (a) and protons (b) as obtained with the Skyrme interaction SLy4 as a function of the quadrupole deformation. Solid (dotted) lines represent levels of positive (negative) parity, and black, red, green, and blue colors represent levels with expectation values of $\langle j_z \rangle = 1/2, 3/2, 5/2$, and $7/2$, respectively.

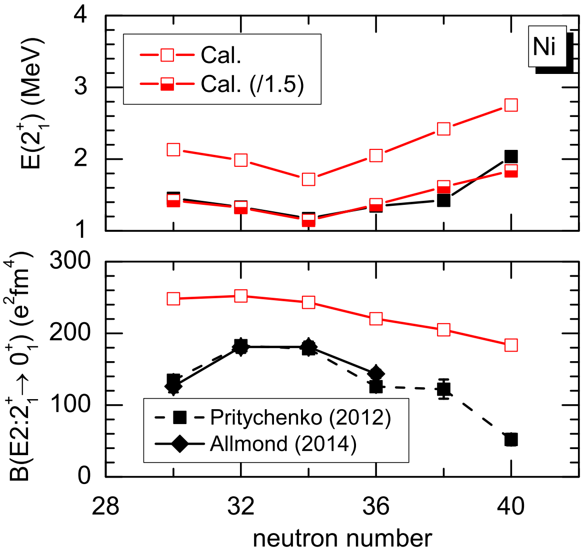

FIG. 14. (Color online) The excitation energy $E(2_1^+)$ of the 2_1^+ state and the $B(E2)$ value for the transition from this state to the ground state for $^{58-68}$Ni. Experimental data are taken from Refs. [94,102].

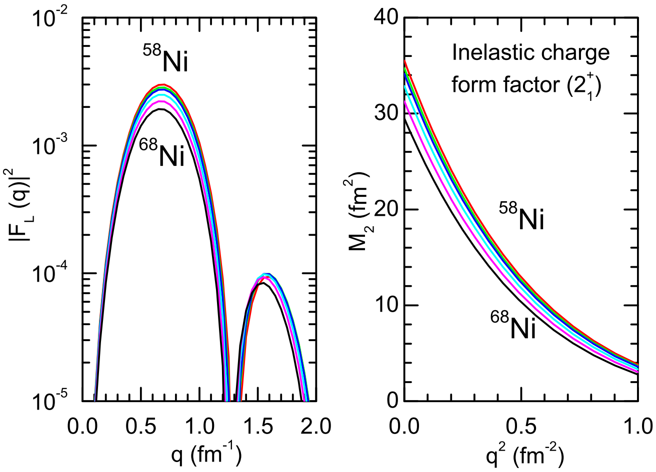

FIG. 15. (Color online) (a) The C2 form factor and (b) the q-dependent transition quadrupole matrix element for the quadrupole transition from the ground state to the 2_1^+ state in $^{58-68}$Ni.

N of the excitation energy of the first 2_1^+ state and of the $B(E2)$ value to the ground state. Although both the $E(2_1^+)$ and $B(E2)$ values are systematically overestimated in our calculation, their evolution as a function of the neutron number is rather well reproduced. We expect that the discrepancy with experiment is mainly due to the time-reversal invariance that is imposed to the mean-field wave functions and that limits the model space of the present calculation to purely collective states. Noncollective time-reversal-invariance-breaking two-quasiparticle excitations are indeed present in the shell-model calculations, which are in better agreement with data. It can be expected that such configurations will decrease the 2^+ excitation energies and make them less collective, resulting in a decrease of the $B(E2)$ values.

The calculated C2 form factor $|F_2(q)|^2$ and the q-dependent transition quadrupole matrix element $M_2(q^2)$ for the quadrupole transition from the ground state to the 2_1^+ state are displayed in Fig. 15. The isotopic dependence of the form factor is very weak, with a decrease of the height of the first maximum with N. The quadrupole transition matrix element $M_2(q)$ at $q \to 0$ decreases in the same way, which corresponds to the smooth decrease of the calculated $B(E2)$ value (cf. Fig. 14).

In Fig. 16, the neutron and proton densities for the transition from the 2_1^+ state to the ground state are shown for $^{58-64}$Ni. The radial profiles are similar for all isotopes, with a large peak at large radii and a smaller one at low values of r. The height of the first peak for the neutron transition density decreases with N and nearly disappears at $N = 40$, in contrast with the second peak.

The ratio η between the values of the quadrupole matrix element for neutrons to that for protons is given in Table I for $^{58-68}$Ni. This ratio provides a measure of the isovector character of the transition. It is close to one in our calculation, indicating that the transitions are predominantly isoscalar.

The radial transition charge density (TCD) from the ground state to the 2_1^+ state is compared to the experimental data [9] for $^{58-68}$Ni in Fig. 17. The shape of the TCD of $^{58-64}$Ni is reproduced by the GCM calculation. However, we overestimate the height of the surface peak and/or the tail part of the TCD. This deficiency can be traced back to the overestimated $B(E2: 2_1^+ \to 0_1^+)$ values, as shown in Fig. 14. In Fig. 18 the GCM inelastic Coulomb form factors $|F_L(q)|^2$ are compared to the experimental data for the transitions from the ground state to the J_1^+ $(L = J = 2,4)$ state. Our calculation reproduces rather well the shapes of the quadrupole and hexadecapole transition form factors, but it systematically underestimates the hexadecapole ones.

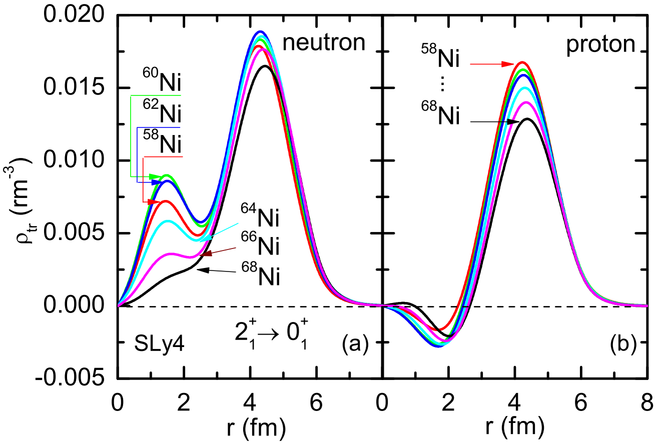

FIG. 16. (Color online) Calculated transition neutron and proton densities from the 2_1^+ state to the ground state for $^{58-68}$Ni.

TABLE I. Isovector character η [cf. Eq. (28)] of the 2_1^+ state of even-even Ni isotopes.

η	^{58}Ni	^{60}Ni	^{62}Ni	^{64}Ni	^{66}Ni	^{68}Ni
This work	1.02	1.05	1.06	1.06	1.03	1.02
Ref. [86]	1.01	1.02	1.12	0.92		
Ref. [103]	1.10	1.31	1.36	1.41		
Ref. [104]	1.10	1.09	1.33	1.02		

V. SUMMARY AND OUTLOOK

We have presented how to determine densities and transition densities, as well as the corresponding form factors, within the beyond-mean-field model that we have developed over many years. The light deformed nucleus ^{24}Mg and the even-mass $^{58-68}$Ni have been used as examples. Depending on the structure of the nucleus, static deformation, or dynamic shape fluctuations, or both might be important for the description of the ground-state and transition densities.

The framework that we have developed is very general and can be applied to any nucleus and any kind of transitions for which calculations using the GCM are available. This gives some hope that applications to odd-mass nuclei will be available in a not too distant future [109]. For a better description of low-lying excited states in spherical even-even nuclei, it would be desirable to add noncollective time-reversal-breaking n-quasiparticle states to the GCM basis.

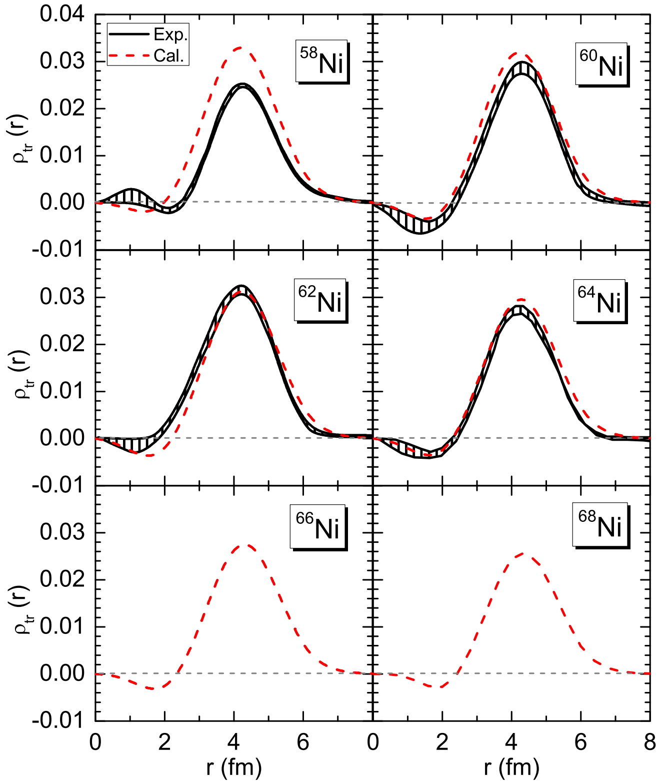

FIG. 17. (Color online) Calculated transition charge densities from the ground state to the 2_1^+ state for $^{58-68}$Ni, in comparison with available data [9].

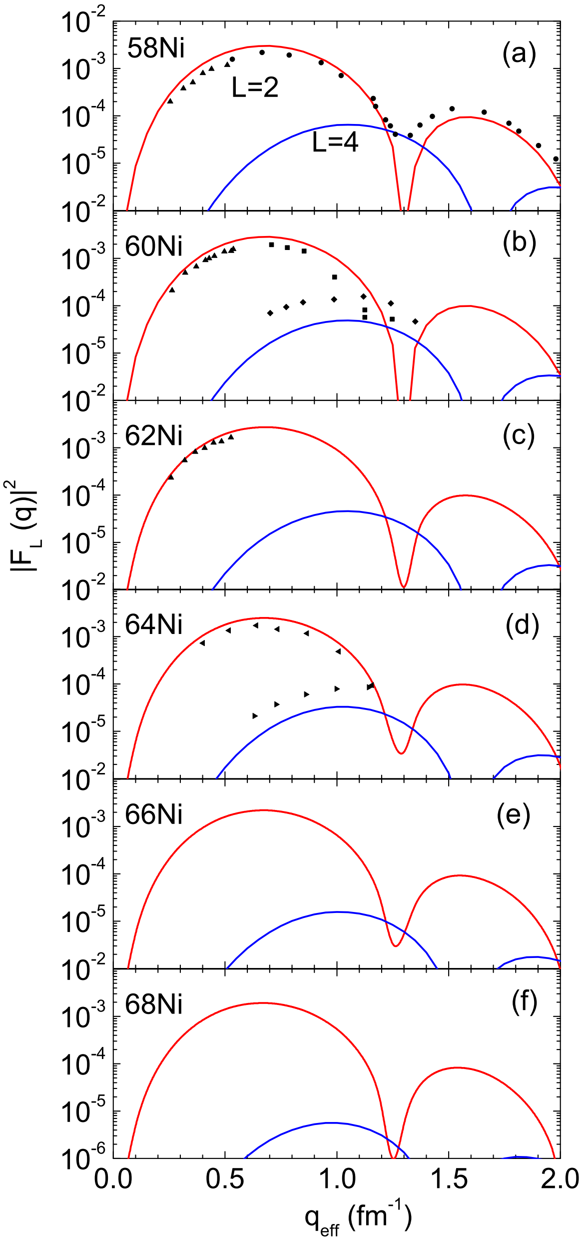

FIG. 18. (Color online) Calculated inelastic Coulomb form factors $|F_L(q)|^2$ for the transition from the ground state to the J_1^+ ($L = J = 2,4$) state in $^{58-68}$Ni, in comparison with available data, taken from Ref. [105] (up triangles), Ref. [106] (squares and diamonds), Ref. [107] (circles), and Ref. [108] (left and right triangles).

Leptonic probes have the advantage that the interaction mechanism and the nucleonic form factors are precisely known, which reduces the theoretical uncertainties. But with additional modeling, also the scattering of hadronic probes off nuclei could be described.

To improve the quality of the results obtained in our model, one certainly needs to construct a new energy functional, which should be adjusted to the data on nuclear charge radii at the beyond-mean-field level. As has been shown in Ref. [110], the charge radii, in particular of light nuclei, become systematically larger in the angular-momentum-projected GCM, which poses a problem when using a parametrization adjusted at the mean-field level. Elastic and inelastic form factors seem to be tools that are very sensitive to the momentum composition of the collective wave functions and should provide stringent tests of nuclear models.

ACKNOWLEDGMENTS

Fruitful discussions with S. Baroni, P.-G. Reinhard, and K. Washiyama are gratefully acknowledged. We also thank H. Mei for critical checking of the formulas for transition densities. This research was supported in part by PAI-P6-23 of the Belgian Office for Scientific Policy, F.R.S.-FNRS (Belgium), the National Science Foundation of China under Grants No. 11305134 and No. 11105111, the European Union's Seventh Framework Programme ENSAR under Grant Agreement No. n262010, and CNRS/IN2P3 through PICS No. 5994.

APPENDIX A: FORM FACTORS OF ELECTRON SCATTERING OFF NUCLEI IN THE PWBA

We suppose that the nucleus makes a transition from the initial state $|\alpha_i\rangle$ to the final state $|\alpha_f\rangle$, where we introduce the shorthand notation α representing $JM\mu$. In the plane-wave Born approximation, the longitudinal form factor, normalized to the nuclear charge Z, is given by the Fourier-Bessel transformation of the transition density $\rho^{\alpha_f}_{\alpha_i}(\mathbf{r})$ [cf. Eq. (11)],

$$|F(\mathbf{q})|^2 = \frac{4\pi}{Z^2\,\hat{J}_i^2} \sum_{M_i,M_f} \left| \sum_{LM} \langle \alpha_f | \hat{M}_{LM} | \alpha_i \rangle Y^*_{LM}(\hat{\mathbf{q}}) \right|^2 . \tag{A1}$$

The multipole operator $\hat{M}_{LM}(q)$ has been defined following Refs. [105,111] as

$$\hat{M}_{LM}(q) \equiv \int d^3r\; j_L(qr)\, Y_{LM}(\hat{\mathbf{r}})\, \hat{\rho}(\mathbf{r}), \tag{A2}$$

where $j_L(qr)$ is a spherical Bessel function and where we have used the relation

$$e^{i\mathbf{q}\cdot\mathbf{r}} = 4\pi \sum_{LM} i^L\, j_L(qr)\, Y^*_{LM}(\hat{\mathbf{q}})\, Y_{LM}(\hat{\mathbf{r}}). \tag{A3}$$

By using the orthogonality of the spherical harmonics, one can show that the radial dependence of $|F(\mathbf{q})|^2$ is given by [3,105,112]

$$|F(q)|^2 = \frac{4\pi}{Z^2 \hat{J}_i^2} \sum_{L=0}^{\infty} |\langle J_f \mu_f || \hat{M}_L(q) || J_i \mu_i \rangle|^2 . \tag{A4}$$

Comparing with Eq. (6), one finds the form factor $F_L(q)$ for an angular momentum transfer L [111]:

$$F_L(q) = \frac{\sqrt{4\pi}}{Z \hat{J}_i} |\langle J_f \mu_f || \hat{M}_L(q) || J_i \mu_i \rangle| . \tag{A5}$$

Using its definition provided by Eq. (A2), the matrix element of the multipole operator $\hat{M}_{LM}$ between an initial $|\alpha_i\rangle$ and a final $|\alpha_f\rangle$ state,

$$\langle \alpha_f | \hat{M}_{LM} | \alpha_i \rangle = \int d^3r\; j_L(qr)\, Y_{LM}(\hat{\mathbf{r}})\, \rho^{\alpha_f}_{\alpha_i}(\mathbf{r}), \tag{A6}$$

is related to the reduced matrix element $\langle J_f; \mu_f || \hat{M}_L(q) || J_i; \mu_i \rangle$ by the Wigner-Eckart theorem [114]

$$\langle J_f \mu_f || \hat{M}_L(q) || J_i \mu_i \rangle = (-1)^{2L}\, \hat{J}_f\, \frac{\langle \alpha_f | \hat{M}_{LM} | \alpha_i \rangle}{\langle J_i M_i L M | J_f M_f \rangle}, \tag{A7}$$

where $\langle J_i M_i L M | J_f M_f \rangle$ is a Clebsch-Gordan coefficient. In other words, one can define a *reduced transition density* $\rho^{J_f,\mu_f}_{J_i,\mu_i,L}(r)$ as a function of radial coordinate r through the 3D transition density $\rho^{\alpha_f}_{\alpha_i}(\mathbf{r})$,

$$\begin{aligned}&\langle \alpha_f | \hat{\rho}(\mathbf{r})\, Y_{LM} | \alpha_i \rangle \\ &\quad = \frac{(-1)^{2L}}{\hat{J}_f} \langle J_i M_i L M | J_f M_f \rangle \langle J_f \mu_f || \hat{\rho}(\mathbf{r}) Y_L || J_i \mu_i \rangle .\end{aligned} \tag{A8}$$

The left-hand side of Eq. (A8) is given by

$$\langle \alpha_f | \hat{\rho}(\mathbf{r}) Y_{LM} | \alpha_i \rangle = \int d\hat{\mathbf{r}}\; \rho^{\alpha_f}_{\alpha_i}(\mathbf{r})\, Y_{LM}(\hat{\mathbf{r}}). \tag{A9}$$

The reduced transition density $\rho^{J_f\mu_f}_{J_i\mu_i,L}(r)$ with angular momentum transfer L is therefore given by

$$\rho^{J_f\mu_f}_{J_i\mu_i,L}(r) = \hat{J}_i^{-1} \langle J_f \mu_f || \hat{\rho}(\mathbf{r})\, Y_L || J_i \mu_i \rangle, \tag{A10}$$

where the factor $\hat{J}_i^{-1}$ is introduced such that the integration of $r^{L+2} \rho^{J_f,\mu_f}_{J_i,\mu_i,L}(r)$ over the radial coordinate r gives the value of the transition matrix element of multipolarity L [cf. Eq. (26)].

In terms of the reduced transition density, the longitudinal form factor $F_L(q)$ for angular momentum transfer L in Eq. (A5) has the form

$$F_L(q) = \frac{\sqrt{4\pi}}{Z} \int_0^{\infty} dr\; r^2\, \rho^{J_f\mu_f}_{J_i\mu_i,L}(r)\, j_L(qr). \tag{A11}$$

We note that our convention for the reduced transition density differs from the one of Eq. (5) of Ref. [76] by a factor of $\sqrt{4\pi}/Z$.

According to the asymptotic behavior of the spherical Bessel function $j_L(qr)$ [4],

$$\begin{aligned}\lim_{qr\to 0} j_L(qr) = \frac{(qr)^L}{(2L+1)!!} \Bigg[1 - \frac{1}{L+3/2} \left(\frac{qr}{2}\right)^2 \\ + \frac{1}{2(L+3/2)(L+5/2)} \left(\frac{qr}{2}\right)^4 - \cdots \Bigg],\end{aligned} \tag{A12}$$

the Coulomb form factor of inelastic scattering in the $q \to 0$ limit is given by [4,113]

$$\begin{aligned}F_L(q) = \frac{\sqrt{4\pi}}{Z} \frac{q^L}{(2L+1)!!} \sqrt{B(EL)} \\ \times \left[1 - \frac{q^2 R_{\mathrm{tr}}^2}{2(2L+3)} + \frac{q^4 R_{\mathrm{tr}}^4}{8(2L+3)(2L+5)} - \cdots \right],\end{aligned} \tag{A13}$$

where the effective transition radii $R^n_{\rm tr}$ ($n=2,4$) are defined as

$$R^n_{\rm tr}=\frac{\int dr\, r^{L+n+2}\,\rho^{J_f\mu_f}_{J_i\mu_i,L}}{\int dr\, r^{L+2}\,\rho^{J_f\mu_f}_{J_i\mu_i,L}}. \tag{A14}$$

From these properties, one can extract the multipolarity L of the transition, the transition strength $B(EL)$, and the transition radius $R^2_{\rm tr}$ from the data for the Coulomb form factor in the low-q region. Usually, one introduces a q-dependent multipole transition matrix element $M^p_L(q)$ for graphical comparisons of matrix elements and Coulomb form factors at small q values:

$$M_L(q^2)=\frac{Z}{\sqrt{4\pi}}\frac{(2L+1)!!}{q^L}F^\ell_L(q). \tag{A15}$$

For elastic scattering, $L=0$, $\alpha_f=\alpha_i=\alpha$, and the Coulomb form factor becomes in the $q\to 0$ limit

$$\begin{aligned}F_0(q)&=\frac{\sqrt{4\pi}}{Z}\int_0^\infty dr\,r^2\,\rho^{J\mu}_{J\mu,0}(r)\,\frac{\sin(qr)}{qr}\\&=1-\frac{q^2}{3!}r^2_{\rm ch}+\cdots,\end{aligned} \tag{A16}$$

where $r_{\rm ch}$ is the rms charge radius of the state $|J\mu\rangle$.

APPENDIX B: DERIVATION OF TRANSITION DENSITY BETWEEN GCM STATES

In this section, we derive the form of the transition density between two arbitrary GCM states for the general case of triaxially deformed nuclei. In this case, the wave function of the GCM state is given by

$$|\alpha\rangle=\sum_{K,q}F^{JK}_{\mu,q}\,\hat P^J_{MK}\,\hat P^N\,\hat P^Z|q\rangle. \tag{B1}$$

Sandwiching the density operator $\hat\rho(\mathbf{r})\equiv\sum_i\delta(\mathbf{r}-\mathbf{r}_i)$ between the wave functions of the initial $|\alpha_i\rangle$ and final $|\alpha_f\rangle$ GCM states, one obtains the 3D transition density

$$\rho^{\alpha_f}_{\alpha_i}(\mathbf{r})=\sum_{K_f,K_i}\sum_{q_f,q_i}F^{J_fK_f*}_{\mu_f,q'}F^{J_iK_i}_{\mu_i,q}\,\rho^{\sigma_fq'}_{\sigma_iq}(\mathbf{r}), \tag{B2}$$

where we have introduced the shorthand notation $\sigma\equiv\{JMK\}$. The kernel of the 3D transition density $\rho^{\sigma_fq'}_{\sigma_iq}(\mathbf{r})$ reads

$$\begin{aligned}\rho^{\sigma_fq'}_{\sigma_iq}(\mathbf{r})=&\frac{\hat J_i^2\,\hat J_f^2}{(8\pi^2)^2}\iint d\Omega'\,d\Omega\,D^{J_f*}_{K_fM_f}(\Omega')\,D^{J_i}_{K_iM_i}(\Omega)\\&\times\langle q'|\hat R(\Omega')\,\hat\rho(\mathbf{r})\,\hat R^\dagger(\Omega')\,\hat P^N\hat P^Z\hat R(\Omega')\,\hat R^\dagger(\Omega)|q\rangle.\end{aligned} \tag{B3}$$

For any HFB state $|q\rangle$, one has

$$\begin{aligned}\langle q'|\hat R(\Omega')\hat\rho(\mathbf{r})\hat R^\dagger(\Omega')|q\rangle&\equiv\langle q'|\hat\rho(\tilde{\mathbf{r}}_{\Omega'})|q\rangle\\&=\hat R^\dagger(\Omega')[\langle q'|\hat\rho(\mathbf{r})|q\rangle],\end{aligned} \tag{B4}$$

where $\tilde{\mathbf{r}}_{\Omega'}=D(\Omega')\,\mathbf{r}$. By decomposing the rotation operator $\hat R(\Omega)\equiv\hat R(\Omega'')\,\hat R(\Omega')$, $\hat R^\dagger(\Omega)=\hat R^\dagger(\Omega')\hat R^\dagger(\Omega'')$ and using the properties of Wigner D functions,

$$D^{J_i}_{K_iM_i}(\Omega)=\sum_K D^{J_i}_{K_iK}(\Omega'')\,D^{J_i}_{KM_i}(\Omega'), \tag{B5}$$

the kernel $\rho^{\sigma_fq'}_{\sigma_iq}(\mathbf{r})$ of the 3D transition density in (B2) can be simplified to

$$\begin{aligned}\rho^{\sigma_fq'}_{\sigma_iq}(\mathbf{r})=&\frac{\hat J_f^2}{8\pi^2}\int d\Omega'\,D^{J_f*}_{K_fM_f}(\Omega')\\&\times\sum_K D^{J_i}_{KM_i}(\Omega')\,\hat R^\dagger(\Omega')\,\rho^{J_iKK_i}_{q'q}(\mathbf{r}),\end{aligned} \tag{B6}$$

where $\rho^{J_iKK_i}_{q'q}(\mathbf{r})$ is defined as

$$\rho^{J_iKK_i}_{q'q}(\mathbf{r})\equiv\langle q'|\hat\rho(\mathbf{r})\hat P^{J_i}_{KK_i}\,\hat P^N\,\hat P^Z|q\rangle. \tag{B7}$$

APPENDIX C: EXPANSION IN TERMS OF SPHERICAL HARMONICS

To separate the radial dependence of the 3D transition density from its trivial angular part, inspired by Ref. [57] we expand $\rho^{J_iKK_i}_{q'q}(\mathbf{r})$ in Eq. (B7) in terms of spherical harmonics,

$$\rho^{J_iKK_i}_{q'q}(\mathbf{r})=\sum_{\lambda=0}^{\infty}\sum_{\nu=-\lambda}^{\lambda}\rho^{J_iKK_i}_{q'q;\lambda\nu}(r)\,Y_{\lambda\nu}(\hat{\mathbf{r}}), \tag{C1}$$

where the radial part $\rho^{J_iKK_i}_{q'q;\lambda\nu}(r)$ is given by

$$\rho^{J_iKK_i}_{q'q;\lambda\nu}(r)=\int d\hat{\mathbf{r}}\;\rho^{J_iKK_i}_{q'q}(r,\hat{\mathbf{r}})\,Y^*_{\lambda\nu}(\hat{\mathbf{r}}). \tag{C2}$$

In this case, the rotation $\hat R^\dagger(\Omega')$ of $\rho^{J_iKK_i}_{q'q}(\mathbf{r})$ in Eq. (B6) can be evaluated analytically as

$$\hat R^\dagger(\Omega')\rho^{J_iKK_i}_{q'q}(\mathbf{r})=\sum_{\lambda\nu\nu'}D^{\lambda*}_{\nu\nu'}(\Omega')\,\rho^{J_iKK_i}_{q'q;\lambda\nu}(r)\,Y_{\lambda\nu'}(\hat{\mathbf{r}}). \tag{C3}$$

The kernel $\rho^{\sigma_fq'}_{\sigma_iq}(\mathbf{r})$ of the 3D transition density in Eq. (B6) becomes

$$\begin{aligned}\rho^{\sigma_fq'}_{\sigma_iq}(\mathbf{r})=&\frac{\hat J_f^2}{\hat J_i^2}\sum_{K\lambda\nu\nu'}\langle J_fK_f\lambda\nu|J_iK\rangle\langle J_fM_f\lambda\nu'|J_iM_i\rangle\\&\times\rho^{J_iKK_i}_{q'q;\lambda\nu}(r)\,Y_{\lambda\nu'}(\hat{\mathbf{r}}),\end{aligned} \tag{C4}$$

where we have expressed the integration of the product of three Wigner D functions over Euler angles as the product of two Clebsch-Gordan coefficients, making the assumption that $J_i+J_f+\lambda$ is integer [114]:

$$\begin{aligned}&\int d\Omega' D^{J_f*}_{K_fM_f}(\Omega')D^{J_i}_{KM_i}(\Omega')D^{\lambda*}_{\nu\nu'}(\Omega')\\&=\frac{8\pi^2}{\hat J_i^2}\langle J_fK_f\lambda\nu|J_iK\rangle\,\langle J_fM_f\lambda\nu'|J_iM_i\rangle.\end{aligned} \tag{C5}$$

By substituting the expression for $\rho^{\alpha_f}_{\alpha_i}(\mathbf{r})$ into Eqs. (A8)–(A10), one finds as an expression for the reduced transition density

$$\begin{aligned}\rho^{J_f\mu_f}_{J_i\mu_i,L}(r)=&(-1)^{2L}\frac{\hat J_f^3}{\hat J_i^3}\sum_{K_f,K_i}\sum_{q'q}F^{J_fK_f*}_{\mu_f,q'}F^{J_iK_i}_{\mu_i,q}\\&\times\sum_{K\lambda\nu\nu'}\langle J_fK_f\lambda\nu|J_iK\rangle\frac{\langle J_fM_f\lambda\nu'|J_iM_i\rangle}{\langle J_iM_iLM|J_fM_f\rangle}\\&\times\rho^{J_iKK_i}_{q'q;\lambda\nu}(r)\int d\hat{\mathbf{r}}\;Y_{LM}(\hat{\mathbf{r}})\,Y_{\lambda\nu'}(\hat{\mathbf{r}}).\end{aligned} \tag{C6}$$

With the help of the orthogonality relation of spherical harmonics, $\int d\hat{\mathbf{r}}\, Y_{LM}(\hat{\mathbf{r}})\, Y_{\lambda\nu'}(\hat{\mathbf{r}}) = (-1)^{-M}\, \delta_{L\lambda}\, \delta_{M-\nu'}$, and the symmetry relation $\langle J_f M_f L - M | J_i M_i \rangle = (-1)^{2L-M+J_i-J_f} \frac{\hat{J}_i}{\hat{J}_f} \langle J_i M_i L M | J_f M_f \rangle$ of the Clebsch-Gordan coefficients, the reduced transition density can be simplified to

$$\rho^{J_f\mu_f}_{J_i\mu_i,L}(r) = (-1)^{J_i-J_f} \frac{\hat{J}_f^2}{\hat{J}_i^2} \sum_{K_f,K_i} \sum_{q'q} F^{J_f K_f *}_{\mu_f,q'} F^{J_i K_i}_{\mu_i,q} \times \sum_{K\nu} \langle J_f K_f L \nu | J_i K \rangle\, \rho^{J_i K K_i}_{q'q;L\nu}(r), \tag{C7}$$

where we have replaced the phase factor $(-1)^{4L-2M+J_i-J_f}$ by $(-1)^{J_i-J_f}$. Substituting Eq. (C2) into the above equation, one finds as the final expression for the reduced transition density of triaxially deformed nuclei

$$\rho^{J_f\mu_f}_{J_i\mu_i,L}(r) = (-1)^{J_i-J_f} \frac{\hat{J}_f^2}{\hat{J}_i^2} \sum_{K_i,K_f} \sum_{q'q} F^{J_f K_f *}_{\mu_f,q'} F^{J_i K_i}_{\mu_i,q} \times \sum_{K\nu} \langle J_f K_f L \nu | J_i K \rangle \int d\hat{\mathbf{r}}\, \rho^{J_i K K_i}_{q'q}(\mathbf{r})\, Y^*_{L\nu}(\hat{\mathbf{r}}). \tag{C8}$$

When axial symmetry about the z axis is imposed on the intrinsic states $|q\rangle$, all components with $K_i \neq 0$ and $K_f \neq 0$ vanish. In this case, the reduced transition density $\rho^{J_f\mu_f}_{J_i\mu_i,L}(r)$ in Eq. (C8) is simplified as

$$\begin{aligned} \rho^{J_f\mu_f}_{J_i\mu_i,L}(r) &= (-1)^{J_i-J_f} \frac{\hat{J}_f^2}{\hat{J}_i^2} \sum_{q'q} F^{J_f 0 *}_{\mu_f,q'} F^{J_i 0}_{\mu_i,q} \\ &\quad \times \sum_{K} \langle J_f 0 L K | J_i K \rangle \int d\hat{\mathbf{r}}\, \rho^{J_i K 0}_{q'q}(\mathbf{r})\, Y^*_{LK}(\hat{\mathbf{r}}) \\ &= (-1)^{J_i-J_f} \frac{\hat{J}_f^2}{\hat{J}_i^2} \sum_{K} \langle J_f 0 L K | J_i K \rangle \\ &\quad \times \int d\hat{\mathbf{r}}\, \rho^{J_f J_i K 0}_{\mu_f \mu_i}(\mathbf{r})\, Y^*_{LK}(\hat{\mathbf{r}}), \end{aligned} \tag{C9}$$

where the *pseudo GCM density* $\rho^{J_f J_i K 0}_{\mu_f \mu_i}(\mathbf{r})$ has been defined in Eq. (19).

APPENDIX D: MULTIPOLE TRANSITION MATRIX ELEMENTS

With the reduced transition density $\rho^{J_f\mu_f}_{J_i\mu_i,L}(r)$ (C8), one can calculate the multipole (L) transition matrix element straightforwardly as

$$\begin{aligned} M^{J_f\mu_f}_{J_i\mu_i,L} &\equiv \int dr\, r^{2+L}\, \rho^{J_f\mu_f}_{J_i\mu_i,L}(r) \\ &= (-1)^{J_i-J_f} \frac{\hat{J}_f^2}{\hat{J}_i^2} \sum_{K_f,K_i} \sum_{q'q} F^{J_f K_f *}_{\mu_f,q'} F^{J_i K_i}_{\mu_i,q} \\ &\quad \times \sum_{K\nu} \langle J_f K_f L - \nu | J_i K \rangle (-1)^{-\nu} \\ &\quad \times \int d^3\mathbf{r}\, r^L\, Y_{L\nu}(\hat{\mathbf{r}})\, \langle q' | \hat{\rho}(\mathbf{r}) \hat{P}^{J_i}_{K K_i} \hat{P}^N \hat{P}^Z | q \rangle. \end{aligned} \tag{D1}$$

By defining the transition operator of multipolarity L as $\hat{Q}_{L\nu} = r^L Y_{L\nu}$, and using the relation between Clebsch-Gordan coefficients and $3j$ symbols [114], we obtain the final expression for the multipole transition matrix element,

$$\begin{aligned} M^{J_f\mu_f}_{J_i\mu_i,L} &= (-1)^{2J_i} \frac{\hat{J}_f^2}{\hat{J}_i} \sum_{K_f,K_i} \sum_{q'q} F^{J_f K_f *}_{\mu_f,q'} F^{J_i K_i}_{\mu_i,q} \\ &\quad \times \sum_{K\nu} (-1)^{J_f-K_f+2K} \begin{pmatrix} J_f & L & J_i \\ -K_f & \nu & K \end{pmatrix} \\ &\quad \times \langle q' | \hat{Q}_{L\nu} \hat{P}^{J_i}_{K K_i} \hat{P}^N \hat{P}^Z | q \rangle. \end{aligned} \tag{D2}$$

It can be easily shown that the electric multipole transition strength is given by

$$B(EL : J_i\mu_i \to J_f\mu_f) = \left| M^{J_f\mu_f,p}_{J_i\mu_i,L} \right|^2, \tag{D3}$$

provided that the operator $\hat{Q}_{L\nu}$ is replaced by the electric one, $\hat{Q}_{L\nu} = e r^L Y_{L\nu}$.

[1] R. Hofstadter, Rev. Mod. Phys. **28**, 214 (1956).

[2] K. Alder, Å. Bohr, T. Huus, B. Mottelson, and A. Winther, Rev. Mod. Phys. **28**, 432 (1956).

[3] T. de Forest, Jr. and J. D. Walecka, Adv. Phys. **15**, 1 (1966).

[4] H. Überall, *Electron Scattering from Complex Nuclei*, Parts A and B (Academic Press, New York, 1971).

[5] R. C. Barrett, Rep. Prog. Phys. **37**, 1 (1974).

[6] B. Dreher, J. Friedrich, K. Merle, H. Rothhaas, and G. Lührs, Nucl. Phys. A **235**, 219 (1974).

[7] T. W. Donnelly and J. D. Walecka, Annu. Rev. Nucl. Part. Sci. **25**, 329 (1975).

[8] J. L. Friar and J. W. Negele, Adv. Nucl. Phys. **8**, 219 (1975).

[9] J. Heisenberg, Adv. Nucl. Phys. **12**, 61 (1981).

[10] J. Heisenberg and H. P. Blok, Annu. Rev. Nucl. Part. Sci. **33**, 569 (1983).

[11] T. W. Donnelly and I. Sick, Rev. Mod. Phys. **56**, 461 (1984).

[12] I. Sick, in *Advanced Methods in the Evaluation of Nuclear Scattering Data*, Lecture Notes in Physics, edited by H. J. Krappe and R. Lipperheide, Vol. 236 (Springer, Berlin, 1985), p. 137.

[13] H. de Vries, C. W. de Jager, and C. de Vries, At. Data Nucl. Data Tables **36**, 495 (1987).

[14] B. Frois and C. N. Papanicolas, Annu. Rev. Nucl. Part. Sci. **37**, 133 (1987).

[15] P. E. Hodgson, Hyperfine Interactions **74**, 75 (1992).

[16] J. D. Walecka, *Electron Scattering for Nuclear and Nucleon Structure* (Cambridge University Press, Cambridge, 2004).

[17] J. Friedrich and N. Voegler, Nucl. Phys. A **373**, 192 (1982).

[18] J. Friedrich, N. Voegler, and P.-G. Reinhard, Nucl. Phys. A **459**, 10 (1986).

[19] M. Wakasugi, T. Suda, and Y. Yano, Nucl. Instrum. Methods Phys. Res., Sect. A **532**, 216 (2004).

[20] T. Suda and M. Wakasugi, Prog. Part. Nucl. Phys. **55**, 417 (2005).
[21] T. Suda *et al.*, Phys. Rev. Lett. **102**, 102501 (2009).
[22] H. Simon, Nucl. Phys. A **787**, 102 (2007).
[23] A. N. Antonov *et al.*, Nucl. Instrum. Methods Phys. Res., Sect. A **637**, 60 (2011).
[24] R. H. Helm, Phys. Rev. **104**, 1466 (1956).
[25] L. J. Tassie, Aust. J. Phys. **9**, 407 (1956).
[26] B. A. Brown, R. Radhi, and B. H. Wildenthal, Phys. Rep. **101**, 313 (1983).
[27] A. E. L. Dieperink, F. Iachello, A. Rinat, and C. Creswell, Phys. Lett. B **76**, 135 (1978); A. E. L. Dieperink, Nucl. Phys. A **358**, 189 (1981).
[28] Y. Horikawa, T. Hoshino, and A. Arima, Nucl. Phys. A **278**, 297 (1977).
[29] H. Sagawa, O. Scholten, and B. A. Brown, Nucl. Phys. A **462**, 1 (1987).
[30] A. Yokoyama and K. Ogawa, Phys. Rev. C **39**, 2458 (1989).
[31] R. A. Radhi and A. Bouchebak, Nucl. Phys. A **716**, 87 (2003).
[32] S. Karataglidis and K. Amos, Phys. Lett. B **650**, 148 (2007).
[33] R. A. Radhi, A. A. Abdullah, and A. H. Raheem, Nucl. Phys. **798**, 16 (2008).
[34] M. Bender, P.-H. Heenen, and P.-G. Reinhard, Rev. Mod. Phys. **75**, 121 (2003).
[35] J. W. Negele, Phys. Rev. C **1**, 1260 (1970).
[36] L. D. Miller and A. E. S. Green, Phys. Rev. C **5**, 241 (1972).
[37] D. Vautherin and D. M. Brink, Phys. Rev. C **5**, 626 (1972).
[38] J. Dechargé and D. Gogny, Phys. Rev. C **21**, 1568 (1980).
[39] Z. Wang and Z. Ren, Phys. Rev. C **70**, 034303 (2004).
[40] A. N. Antonov, D. N. Kadrev, M. K. Gaidarov, E. Moya de Guerra, P. Sarriguren, J. M. Udias, V. K. Lukyanov, E. V. Zemlyanaya, and G. Z. Krumova, Phys. Rev. C **72**, 044307 (2005).
[41] X. Roca-Maza, M. Centelles, F. Salvat, and X. Viñas, Phys. Rev. C **78**, 044332 (2008).
[42] X. Roca-Maza, M. Centelles, F. Salvat, and X. Viñas, Phys. Rev. C **87**, 014304 (2013).
[43] J. W. Negele and G. Rinker, Phys. Rev. C **15**, 1499 (1977).
[44] E. Moya de Guerra, Ann. Phys. (NY) **128**, 286 (1980).
[45] P. Sarriguren, E. Graca, D. W. L. Sprung, E. Moya de Guerra, and D. Berdichevsky, Phys. Rev. C **40**, 1414 (1989).
[46] D. Berdichevsky, P. Sarriguren, E. Moya de Guerra, M. Nishimura, and D. W. L. Sprung, Phys. Rev. C **38**, 338 (1988).
[47] A. Faessler, S. Krewald, A. Plastino, and J. Speth, Z. Phys. A **276**, 91 (1976).
[48] P.-G. Reinhard and S. Drechsel, Z. Phys. A **290**, 85 (1979).
[49] D. Gogny, in *Nuclear Physics with Electromagnetic Interactions*, edited by H. Arenhövel and D. Drechsel, Lecture Notes in Physics, Vol. 108 (Springer-Verlag, New York, 1979), p. 88.
[50] J. Dechargé, M. Girod, D. Gogny, and B. Grammaticos, Nucl. Phys. A **358**, 203 (1981).
[51] H. Esbensen and G. F. Bertsch, Phys. Rev. C **28**, 355 (1983).
[52] F. Barranco and R. A. Broglia, Phys. Rev. Lett. **59**, 2724 (1987).
[53] M. B. Johnson and G. Wenes, Phys. Rev. C **38**, 386 (1988).
[54] T. Sil and S. Shlomo, Phys. Scr. **78**, 065202 (2008).
[55] G. P. A. Nobre, F. S. Dietrich, J. E. Escher, I. J. Thompson, M. Dupuis, J. Terasaki, and J. Engel, Phys. Rev. C **84**, 064609 (2011).
[56] Y. Abgrall, P. Gabinski, and J. Labarsouque, Nucl. Phys. A **232**, 235 (1974).
[57] Z. Zaringhalam and J. W. Negele, Nucl. Phys. A **288**, 417 (1977).
[58] E. Moya de Guerra and A. E. L. Dieperink, Phys. Rev. C **18**, 1596 (1978).
[59] E. Moya de Guerra and S. Kowalski, Phys. Rev. C **20**, 357 (1979); **22**, 1308 (1980).
[60] A. E. L. Dieperink and E. Moya de Guerra, Phys. Lett. B **189**, 267 (1987).
[61] E. Graca, P. Sarriguren, D. Berdichevsky, D. W. L. Sprung, E. Moya De Guerra, M. Nishimura, Nucl. Phys. A **483**, 77 (1988).
[62] M. Nishimura, D. W. L. Sprung, and E. Moya De Guerra, Phys. Lett. B **161**, 235 (1985).
[63] E. Moya de Guerra, Phys. Rep. **138**, 293 (1986).
[64] J. M. Yao, S. Baroni, M. Bender, and P.-H. Heenen, Phys. Rev. C **86**, 014310 (2012).
[65] J. M. Yao, H. Mei, and Z. P. Li, Phys. Lett. B **723**, 459 (2013).
[66] X. Y. Wu, J. M. Yao, and Z. P. Li, Phys. Rev. C **89**, 017304 (2014).
[67] H. Mei, K. Hagino, J. M. Yao, and T. Motoba, Phys. Rev. C **90**, 064302 (2014).
[68] Y. Fukuoka, S. Shinohara, Y. Funaki, T. Nakatsukasa, and K. Yabana, Phys. Rev. C **88**, 014321 (2013).
[69] J. Terasaki, P.-H. Heenen, H. Flocard, and P. Bonche, Nucl. Phys. A **600**, 371 (1996).
[70] P. Bonche, H. Flocard, and P.-H. Heenen, Comput. Phys. Commun. **171**, 49 (2005).
[71] E. Chabanat, P. Bonche, P. Haensel, J. Meyer, and R. Schaeffer, Nucl. Phys. A **635**, 231 (1998); **643**, 441(E) (1998).
[72] C. Rigollet, P. Bonche, H. Flocard, and P.-H. Heenen, Phys. Rev. C **59**, 3120 (1999).
[73] P. Ring and P. Schuck, *The Nuclear Many-Body Problem* (Springer, Heidelberg, 1980).
[74] D. Lacroix, T. Duguet, and M. Bender, Phys. Rev. C **79**, 044318 (2009).
[75] M. Bender and P.-H. Heenen, Phys. Rev. C **78**, 024309 (2008).
[76] J. Heisenberg, J. Lichtenstadt, C. N. Papanicolas, and J. S. McCarthy, Phys. Rev. C **25**, 2292 (1982).
[77] I. Angeli, At. Data Nucl. Data Tables **87**, 185 (2004).
[78] K. W. Schmid and F. Grümmer, Z. Phys. A **337**, 267 (1990).
[79] K. W. Schmid and P.-G. Reinhard, Nucl. Phys. A **530**, 283 (1991).
[80] R. R. Rodríguez-Guzmán and K. W. Schmid, Eur. Phys. J. A **19**, 45 (2004).
[81] L. J. Tassie and F. C. Barker, Phys. Rev. **111**, 940 (1958).
[82] J. M. Yao, J. Meng, P. Ring, and D. Vretenar, Phys. Rev. C **81**, 044311 (2010); J. M. Yao, K. Hagino, Z. P. Li, J. Meng, and P. Ring, *ibid.* **89**, 054306 (2014).
[83] T. R. Rodríguez and J. L. Egido, Phys. Rev. C **81**, 064323 (2010).
[84] D. Baye and P.-H. Heenen, J. Phys. A **19**, 2041 (1986).
[85] A. Valor, P. H. Heenen, and P. Bonche, Nucl. Phys. A **671**, 145 (2000).
[86] Y. Terrien, Nucl. Phys. A **199**, 65 (1973); **215**, 29 (1973).
[87] R. Rodríguez-Guzmán, J. L. Egido, and L. M. Robledo, Nucl. Phys. A **709**, 201 (2002).
[88] T. Nikšić, D. Vretenar, and P. Ring, Phys. Rev. C **73**, 034308 (2006); **74**, 064309 (2006).
[89] G. C. Li, M. R. Yearian, and I. Sick, Phys. Rev. C **9**, 1861 (1974).

[90] A. Johnston and T. E. Drake, J. Phys. A **7**, 898 (1974).
[91] H. Zarek *et al.*, Phys. Lett. B **80**, 26 (1978).
[92] J. N. Orce, B. Crider, S. Mukhopadhyay, E. Peters, E. Elhami, M. Scheck, B. Singh, M. T. McEllistrem, and S. W. Yates, Phys. Rev. C **77**, 064301 (2008).
[93] R. Broda *et al.*, Phys. Rev. C **86**, 064312 (2012).
[94] J. M. Allmond *et al.*, Phys. Rev. C **90**, 034309 (2014).
[95] R. F. Simoes, D. S. Monteiro, L. K. Ono, A. M. Jacob, J. M. B. Shorto, N. Added, and E. Crema, Phys. Lett. B **527**, 187 (2002).
[96] A. M. Stefanini *et al.*, Phys. Rev. Lett. **74**, 864 (1995).
[97] P. E. Garrett and J. L. Wood, J. Phys. G **37**, 064028 (2010).
[98] P. E. Garrett, K. L. Green, and J. L. Wood, Phys. Rev. C **78**, 044307 (2008).
[99] J. R. Ficenec, W. P. Trower, J. Heisenberg, and I. Sick, Phys. Lett. B **32**, 460 (1970).
[100] I. Sick, J. B. Bellicard, M. Bernheim, B. Frois, M. Huet, Ph. Leconte, J. Mougey, X.-H. Phan, D. Royer, and S. Turck, Phys. Rev. Lett. **35**, 910 (1975).
[101] M. Girod and D. Gogny, Phys. Lett. B **64**, 5 (1976).
[102] B. Pritychenko, J. Choquette, M. Horoi, B. Karamy, and B. Singh, At. Data Nucl. Data Tables **98**, 798 (2012).
[103] A. Chaumeaux, V. Layly, and R. Schaeffer, Ann. Phys. (NY) **116**, 247 (1978).
[104] R. M. Lombard, G. D. Alkhazov, and O. A. Domchenkov, Nucl. Phys. A **360**, 233 (1981).
[105] M. A. Duguay, C. K. Bockelman, T. H. Curtis, and R. A. Eisenstein, Phys. Rev. **163**, 1259 (1967).
[106] Y. Torizuka, Y. Kojima, M. Oyamada, K. Nakahara, K. Sugiyama, T. Terasawa, K. Itoh, A. Yamaguchi, and M. Kimura, Phys. Rev. **185**, 1499 (1969).
[107] B. Frois *et al.*, Phys. Lett. B **122**, 347 (1983).
[108] M. R. Braunstein, J. J. Kraushaar, R. P. Michel, J. H. Mitchell, R. J. Peterson, H. P. Blok, and H. de Vries, Phys. Rev. C **37**, 1870 (1988).
[109] B. Bally, B. Avez, M. Bender, and P.-H. Heenen, Phys. Rev. Lett. **113**, 162501 (2014).
[110] M. Bender, G. F. Bertsch, and P.-H. Heenen, Phys. Rev. C **78**, 054312 (2008).
[111] R. Raphael and M. Rose, Phys. Rev. C **1**, 547 (1970).
[112] J. L. Friar and W. C. Haxton, Phys. Rev. C **31**, 2027 (1985).
[113] M. Rosen, R. Raphael, and H. Überall, Phys. Rev. **163**, 927 (1967).
[114] D. A. Varshalovich, A. N. Moskalev, and V. K. Khersonskii, *Quantum Theory of Angular Momentum* (World Scientific, Singapore, 1988).